5-1973

The Formation and Properties of Machining Burrs

LaRoux K. Gillespie
Utah State University

THE FORMATION AND PROPERTIES OF MACHINING BURRS

by

LaRoux K. Gillespie

A thesis submitted in partial fulfillment
of the requirements for the degree

of

MASTER OF SCIENCE

in

Manufacturing Engineering

UTAH STATE UNIVERSITY
Logan, Utah

1973

ACKNOWLEDGMENTS

This study of Burr Formation is an outgrowth of the author's earlier work on Deburring Processes. In studying the techniques required for removing burrs from precision miniature components two important considerations became obvious: a) For repeatible deburring the burr properties have to be repeatible and b) A knowledge of how burrs form is essential if one wishes to predict deburring requirements and minimum cost machining-deburring conditions.

In order to establish the generality of the Burr Formation Mechanisms the four principle machining operations (drilling, milling, turning, and grinding) were studied. The Burr Formation Mechanisms and resulting properties are described analytically and empirically.

The author is indebted to the Bendix Corporation for providing the time to pursue this study and for the graduate fellowship which made it possible to return to graduate study. The many excellent suggestions from Dr. P. T. Blotter, Dr. Carl D. Spear, and Professor W. Karl Somers provided many of the links required to tie the theory and empirical results together. Robert Poor's assistance in making the 1000 burr measurements is also gratefully acknowledged.

Finally, I owe a special debt of gratitude to my wife who stood patiently by while her husband engrossed himself in this study.

LaRoux K. Gillespie

TABLE OF CONTENTS

LIST OF TABLES

LIST OF TABLES (Continued)

LIST OF TABLES (Continued)

LIST OF FIGURES

LIST OF FIGURES (Continued)

LIST OF FIGURES (Continued)

LIST OF FIGURES (Continued)

DEFINITION OF TERMS AND SYMBOLS

b - width of cut

BHN - Brinell Hardness Number

BUE - built up edge

C - machining constant, different for each material

d - radial depth of cut in milling

df - degrees of freedom

E - modulus of elasticity

f - feedrate in inches per revolution

F_c - main cutting force

F_a - feed force (in direction of tool motion)

F_r - thrust force (in radial direction)

H - material hardness

M_b - bending moment

MHN - Meyer Hardness Number

n - strain hardening exponent

n' - Meyer Strain Hardenability Exponent

SCEA - Side Cutting Edge Angle

t - depth of cut in turning

t_i - instantaneous depth of cut

V - cutting velocity (in surface feet per minute)

α - clearance angle

γ - rake angle

ϵ - true strain

ϵ_f - true strain at fracture (in tensile test)

Θ_H - Helix Angle

Θ_P - point angle on a drill

u - coefficient of friction

ν - Poisson's Ratio (0.5 for plastic materials)

ρ - radius of curvature

σ_e - stress at the elastic limit

σ_o - strain hardening constant

σ_p - plastic stress

σ_s - shear stress

τ - friction angle

ϕ - plasticity angle relating tangential to radial stress

ϕ_a - plasticity angle at radius a

ϕ_s - shear angle

ABSTRACT

The Formation and Properties

of Machining Burrs

by

LaRoux K. Gillespie, Master of Science

Utah State University, 1973

Major Professor: Dr. Carl D. Spear
Department: Manufacturing Engineering

The formation of burrs in Machining Operations occurs by three Basic Mechanisms:

1) Lateral extrusion of material

2) Bending of the chip

3) Tearing of the chip from the workpiece

Each of these mechanisms has been studied analytically and compared to experimental results. The agreement between predictions and measurements has been found to be close.

Drilling, milling, grinding, and turning burrs were produced in 303Se stainless steel and their properties were related to tool geometry, feedrates, and depth of cut. One thousand measurements were made and subsequently analyzed by analysis of variance techniques. The properties measured include burr length and thickness.

Both the theory and the empirical results indicate that burrs cannot be prevented by changing machining variables. Burr size can be minimized, however, by appropriate machining conditions.

(165 pages)

INTRODUCTION

Statement of the problem

One of the chronic problem areas in manufacturing is the removal of machining burrs. Industry annually spends five billion dollars to remove these burrs. The deburring workers impale themselves daily in their deburring tools, and many of the overlooked burrs jam gear boxes or precision assemblies, and otherwise impede part function.

Although a considerable amount of money has been spent developing improved deburring methods, little energy has been applied to minimizing burrs. Similarly few individuals have attempted to predict or measure burr properties. ASTME (1), Biegel and Holmes(3) Buhler and Pollmar(5), Hugo (18), Strasser (33), Wang (38) and Wukusik (39) have analyzed burr heights produced in punching. Each of these investigations, however, ignored burr thickness and burr hardness which are more significant than burr height in burr removal operations. McBride (22) documents burr sizes produced by EDM. Zaima, Yuki, and Kamo (40) present burr height data for drilling. The author has developed burr heights, thickness, and hardness data for milling, drilling, turning, and grinding of several materials (12, 13, 14, 15). In none of these studies however has an attempt been

made to define analytically the mechanism of burr formation. This study was designed to provide such analytical models.

A knowledge of burr formation mechanics is particularly acute in those industries producing precision miniature components. Typical burrs are often five to ten times thicker than the total tolerance on the part. In such applications it is not unusual for burr removal costs to equal the cost of machining the part. The ability to preselect conditions producing smaller burrs will thus greatly minimize deburring costs.

Objective of the study

The objective of this study is to identify how machining burrs form and to present methods for predicting burr properties. These results will allow others to determine how to produce the most easily removable burrs.

Specifically this study will:

A) Determine how burrs are generated.

B) Determine how such machining parameters as feed rates, tool geometry and tool wear affect burr properties.

C) Develop analytical techniques for predicting burr properties.

Method of approach

The approach used in this study was to

A) Analyze how burrs form in the drilling, milling, turning, and grinding processes.

B) Develop the analytical equations describing burr formation. These equations were to be general enough to apply to any workpiece material.

C) Perform machining tests to determine the actual magnitudes of burrs formed and the effects of feedrate, depth of cut, tool geometry and tool wear. These tests were performed on 303Se stainless steel workpieces.

Elementary plasticity concepts were used to develop the analytical equations. Factorial analysis was used to determine the effects of the machining parameters on the burr properties. Because of the very minute size and position of the normal burrs, high speed motion pictures of the formation mechanisms could not be employed as originally planned.

BASIC MECHANISMS OF BURR FORMATION

There are four basic types of burr. These basic types are:

A) The Poisson Burr

This burr is a result of a material's tendancy to bulge at the sides when the material is compressed. In the case of the Poisson Burr the material is compressed until permanent plastic deformation occurs. The name 'Poisson Burr' is derived from Poisson's Ratio (ν) which accounts for lateral deformation of materials.

B) The Roll-Over Burr

This burr is essentially a chip which is pushed out of the cutter's path rather than sheared. It is the long burr found at the end of a cut.

C) The Tear Burr

The Tear Burr is the result of material tearing loose from the workpiece rather than shearing. It is similar to the burr formed in punching operations.

D) The Cut-Off Burr

This burr is a result of workpiece separation from the raw material before the separation cut is finished. This burr which is actually material which has not been cut is

frequently found on saw cuts and on automatic screw machine parts. Since this burr can be readily prevented by supporting the part until complete cut off is achieved it was not included in this study.

It is possible for some burrs to be a combination of the above types. In most situations however, one mode of formation will predominate.

To visualize the mechanics of Poisson Burr formation one must recognize two significant factors:

A) The actual cutting edge of the tool is not perfectly sharp. It has a small radius on it. (Figure 1) In addition the built up edge (BUE) which frequently occurs in metal cutting creates a much larger effective cutting edge radius. Form and Beglinger (10) indicate that even in free machining, material accumulates in front of the tool which would also cause a larger effective cutting edge radius than physically exists on the tool.

B) High pressures can exist on the flank surface of the tool. (Figure 2) These pressures are particularly noticeable on materials with low thermal conductivity, high coefficients of thermal expansion and low modulus of elasticity.

Since the material ahead of the tool sees the cutting edge as a radius, it is convenient to treat the cutting edge as a long, thin cylinder. As shown in Figure 3, when a cylinder is pushed into a workpiece

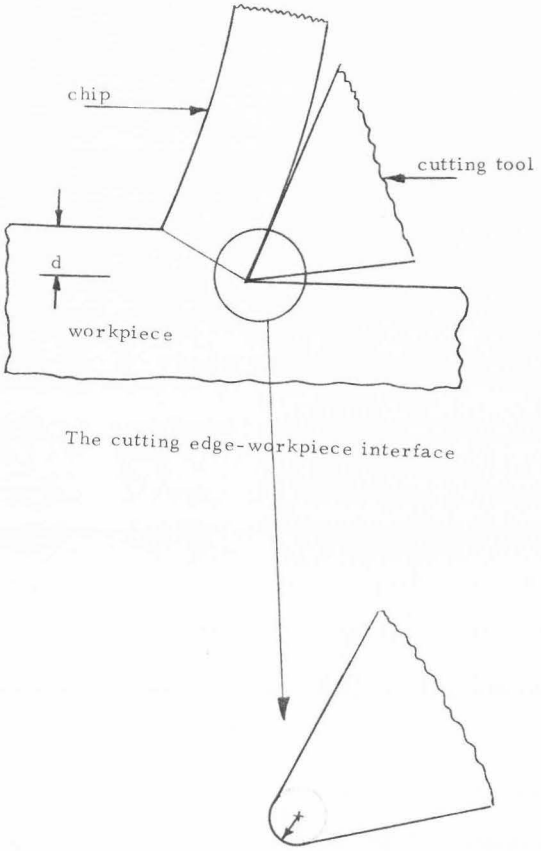

Figure 1. Schematic illustration of the cutting edge.

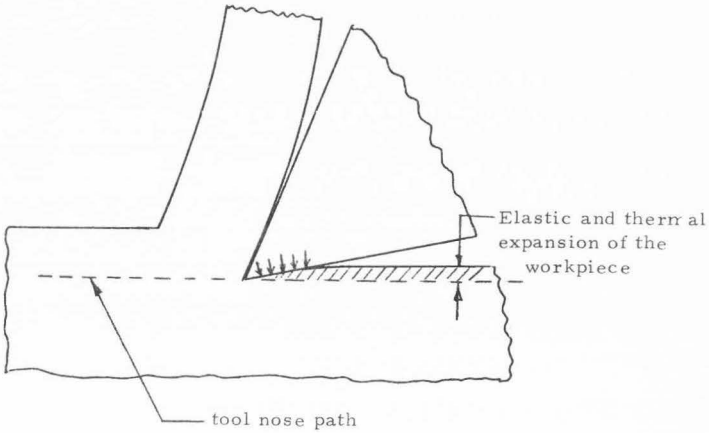

Figure 2. Pressures on flank surface.

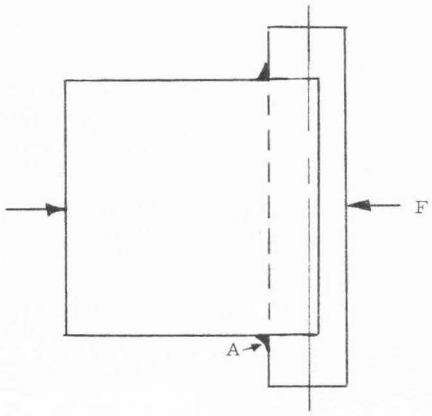

Top View

(a)

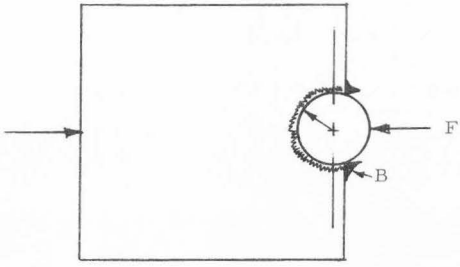

Side view

(b)

Figure 3. Bulging caused by indentation of cylinder.

bulging occurs at the edges of the workpiece. The magnitude of this bulge is a function of the effective cutting edge radius, the pressure between the effective radius and the material properties. When the cylinder is pushed into the workpiece to a depth of r the burr has reached its maximum size. As the cylinder continues to advance through the material the burr is generated along all surfaces which were in contact with the cylinder. (Figure 3b) One obvious requirement for the formation of the Poisson Burr is that the cutting edge must extend beyond the edge of the workpiece. With the exception of plunge cuts this criteria is met on most machining operations.

The equations derived in Appendix A indicate that the burr thickness produced by the cutting edge radius is

$$w = a\left[e^{-\sqrt{3}\phi_a}\cos\phi_a - 1\right] \qquad [1]$$

where

$$\phi_a = -\sin^{-1}\left(\frac{\sqrt{3}P}{2\sigma_a}\right) + \frac{\pi}{6} \qquad [2]$$

and

a = effective cutting edge radius

P = pressure at effective cutting edge radius

σ_a = yield stress of a perfectly plastic material

c = burr thickness

the burr length is

$$\Delta h = \left[\frac{h\,(1+\nu)}{\sqrt{3}\ E}\,\sigma_a\ e^{-\sqrt{3}\,\phi_a}\right]\left[\frac{\sin\phi}{2\sqrt{3}\,(\cos\phi + \sin\phi)}\right] \qquad [3]$$

where

Δh = burr length

ν = Poisson's ratio

E = modulus of elasticity

h = length of cutter engaged in material

ϕ = state of plastic flow defined by Figure 10 in Appendix A.

Thus from [3] the burr length is seen to depend upon the length of tool in the cut, Poisson's ratio, and the yield stress. It is inversely proportional to the modulus of elasticity. The effect of P is somewhat obscured, but from [2] as P gets larger, ϕ_a becomes more negative. Thus increasing P increases the burr height.

A tacit assumption made in the above analysis is that the depth of cut is sufficient such that material does not flow easily toward the chip side of the cut. In the case of small depths of cut this assumption is not justified. The Poisson Burr in this case forms as a result of the high pressures on the flank surface. There is no appreciable burr formed at the nose of the tool. In a material which strain hardens, the material behind the contact area (Figure 2) has a much higher resistance to flow than the material near the area of contact. This

higher resistance is a result of the strain hardening which it has just undergone. The easiest deformation path for the material at the contact area is to flow vertically out the sides of the workpiece. This material therefore becomes a burr.[1] If a tool is allowed to dwell in a cut the burr may increase in size because of the pressures on the flank surface.

The effects of strain hardening are perhaps more easily appreciated by a consideration of the following equation for strain hardening.

$$\sigma = \sigma_o \epsilon^n \qquad [4]$$

where

σ is the true stress in the plastic region

σ_o is a material constant

ϵ is the true strain in the workpiece

n is the strain hardening exponent

Equation [4] essentially states that the true yield stress of a material increases as the material is strained. The true strain ϵ is typically less than 1.0 and n varies from 0 to 0.5. Thus once a material has been strained plastically it takes a much higher stress to cause it to flow plastically again.

Figure 3b illustrates another type of Poisson Burr which

---

[1] For this study a burr is defined as any material which was not originally at that position and which is not a desired part of the workpiece. It is recognized however that burrs can be a desirable part of the workpiece in some instances. (See for example, Crane (6))

occurs as the cutter enters the workpiece. In this case the Poisson Burr is formed in the direction opposite the tool motion. In the cases described above, the burr was formed at right angles to the direction of tool motion. As the cylinder is pressed into the workpiece the displaced material moves out along the free surface. The magnitude of this entrance burr is inversely related to the material's strain hardening exponent. Although a rigorous analysis has not been made of this formation mode it would appear to be similar to the modes occuring when spherical indenties are pressed into a workpiece. Figure 4 presents the results of measurements on spherical indentations.[1] The significance of Figure 4 is readily apparent--materials with strain hardening exponents of .30 or greater will not form entrance burrs. As indicated by the negative values of ridge height an edge rounding occurs for values of n greater than .30.

The Roll-Over Burr is one of the most visable types of burrs. As shown in Figure 5, in an end milling operation, the burr is as long as the radial depth of cut d. Its height is equal to the axial depth of cut. It forms in any operation in which the principal cutting force passes over a free edge.

---

[1] The indentation phemmenon and the data plotted in Figure 4 are discussed more fully in Appendix A.

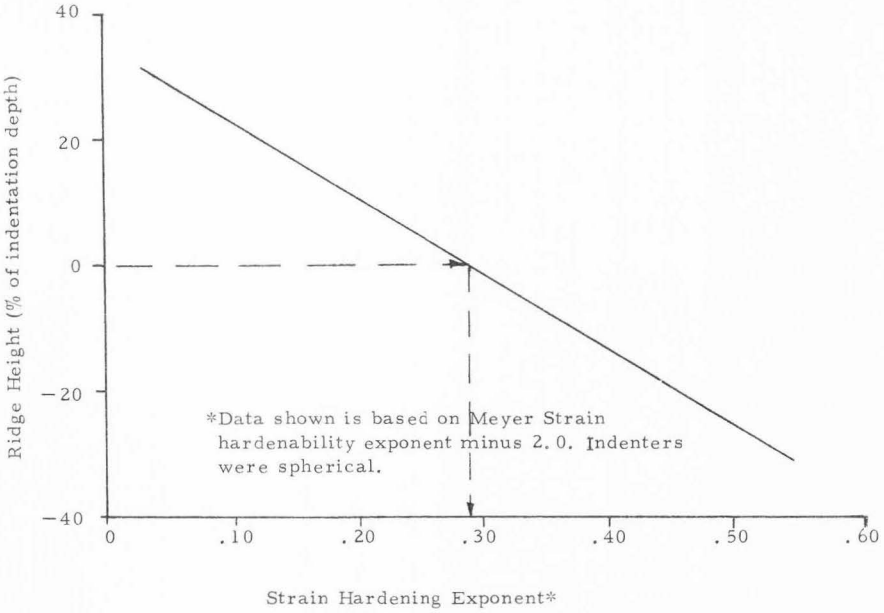

Figure 4. Effect of strain hardening exponent on ridging.

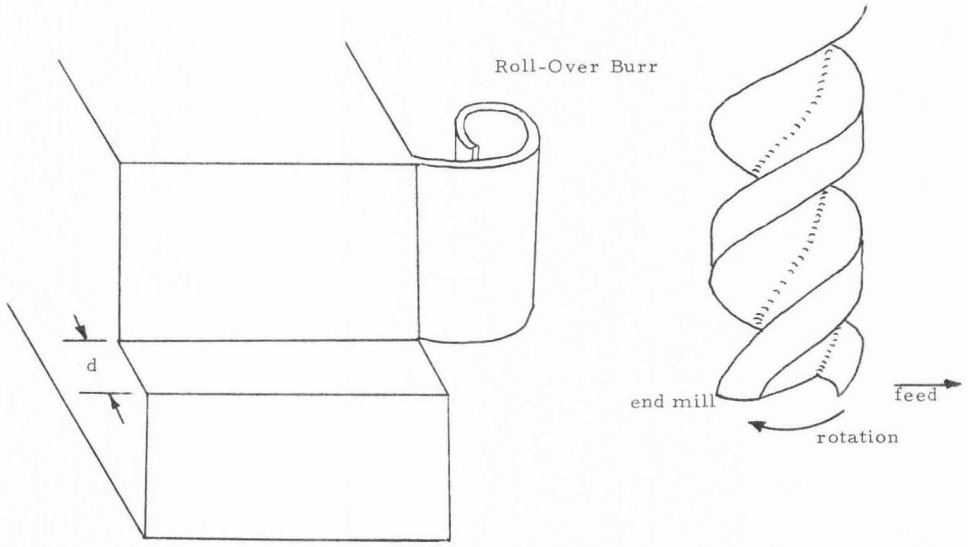

Figure 5. Illustration of a Roll-Over Burr produced by end mill

This burr will only form on ductile materials. As shown in Figure 6 when the tool nears the end of a cut a bistable condition occurs. The first possibility is that the chip will be sheared off the workpiece in the same fashion as occurred throughout the cut. The second possibility is that the chip will bend out of the way of the tool. In this second possibility the bending occurs similar to a plastic hinge. The thickness of this burr is found analytically by equating the energy required to bend a beam of thickness 2h to the work required to cut a chip whose length is 2h. The resulting expression is solved for 2h. As shown in Appendix A for a perfectly plastic material in orthoginal turning the resulting equation is

$$2h = \left[2Fc + \sqrt{4F_c^2 - 2b\sigma_e\Theta t}\right] \frac{1}{b\sigma_e\Theta} \qquad [5]$$

The maximum value for 2h is

$$2h = \frac{4F_c}{b\sigma_e\Theta} = \frac{4t\sigma_s}{\sigma_e\Theta} \text{ (function of angles)} \qquad [6]$$

where

F_c = principal cutting force

b = length of cut

σ_e = stress at elastic limit

σ_s = shear strength of the workpiece

Θ = angle through which chip is bent (90^o + rake angle)

t = depth of cut

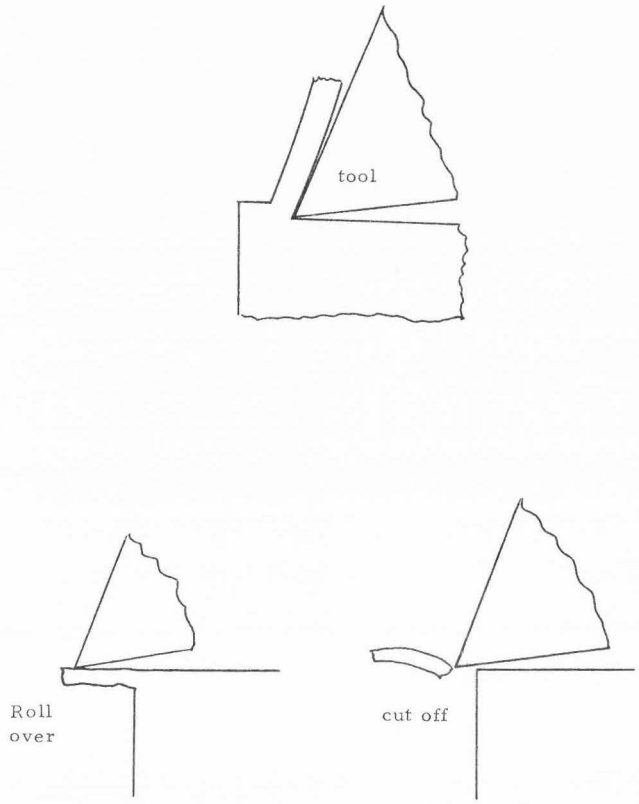

Figure 6. Roll-Over Burr.

As seen in equation [6], the burr thickness increases anytime the cutting force increases. Thus dull cutters will increase burr thickness. Shallow depths of cut and large rake angles will reduce burr size.

The determination of whether or not a Roll Over Burr will occur can be made using the following inequality,

$$\epsilon_{max} \leq \epsilon_f \qquad [7]$$

where

$$\epsilon_{max} = \left(\frac{\epsilon_f^{\,n}\,\Theta}{n+2} \right)^{\frac{1}{n+1}} \qquad [8]$$

ϵ_{max} = maximum true strain in the bent beam

ϵ_f = true strain at fracture (of a tensile specimen)

Θ = 90^{o} rake angle

n = strain hardening exponent

Thus if ϵ_{max} in equation [8] is greater than ϵ_f the burr will fracture before it is bent out of the cutter's path.

The hardness of a material is a function of the amount of strain hardening. Using the Meyer Hardness Number (MHN) for example,

$$MHN = 2.8\,\sigma_o\,\epsilon^n \qquad [9]$$

Thus for any given strain in any given material the hardness is predictable. Since the strain in bending varies linearly across the beam cross section, the average strain is

$$\bar{\epsilon} = \frac{\epsilon_o + \epsilon_{max}}{2} \qquad [10]$$

Where ϵ_o is the initial strain at the center of the beam (or chip or burr). The average hardness then across the Roll-Over Burr is

$$\bar{H} = \frac{H_o + H_{max}}{2} \qquad [11]$$

where

$\bar{H}$ = the average hardness expressed in any hardness system

H_o = hardness of the initial material

H_{max} = hardness at a strain of ϵ_{max}

Milling operations frequently produce a burr which is the result of material tearing when a side milling cutter is narrower than the workpiece, the chip is separated from the workpiece as shown in Figures 7 and 8. The initial entrance of the tool into the workpiece produces a small cavity. As that tooth continues its cut the cavity becomes bigger. The material connecting the chip to the workpiece continues to stretch until it fractures. Intuitively one expects the fracture to occur midway between the chip and the workpiece. The burr than is that portion of stretched metal which remains on the workpiece.

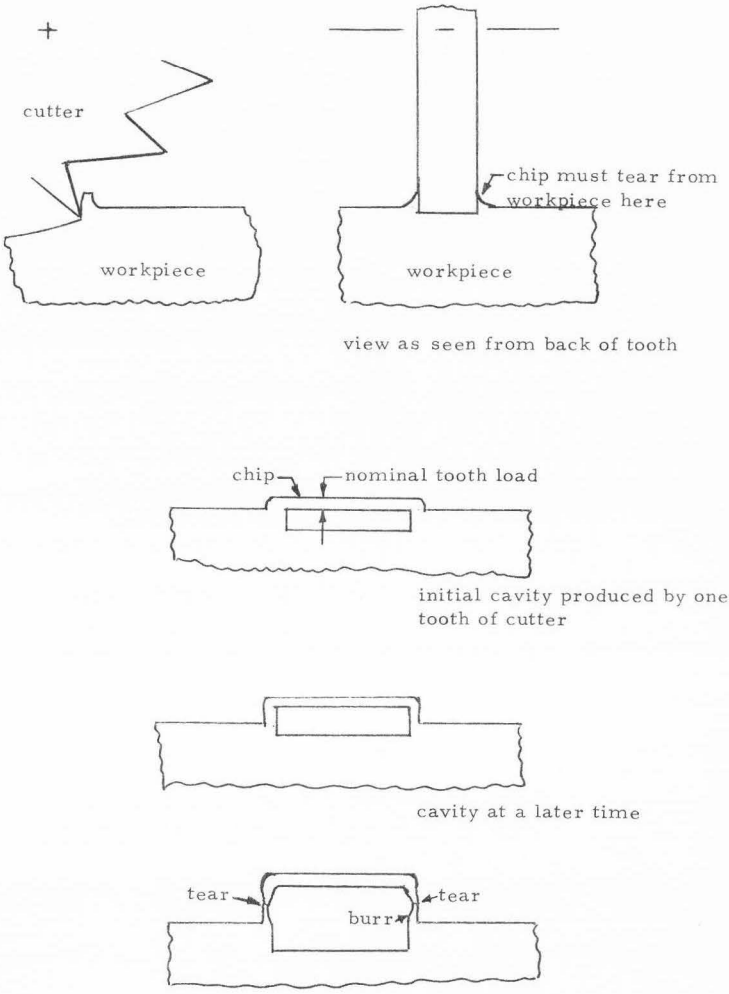

Figure 7. Simplified illustration of burr formation in orthoginal milling.

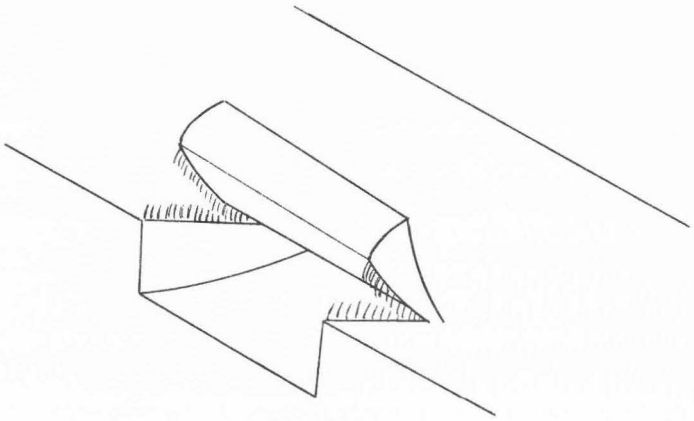

Figure 8. Separation of initial chip in side milling.

Although this description of Tear Burr formation illustrates the basic phenomena which occurs, it ignores the effects of chip compression. If the chip shears along planes are shown in Figure 9b then the slippage along the planes shown will noticeably influence the burr at the edge of the tool.

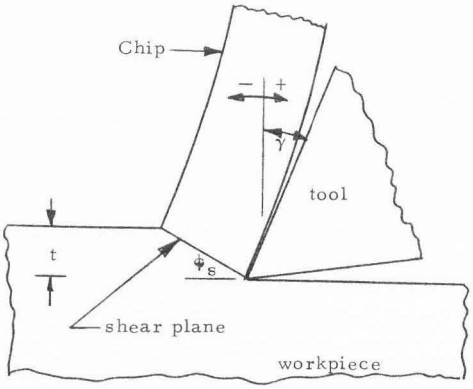

Schematic illustration of the orthogonal machining process

(a)

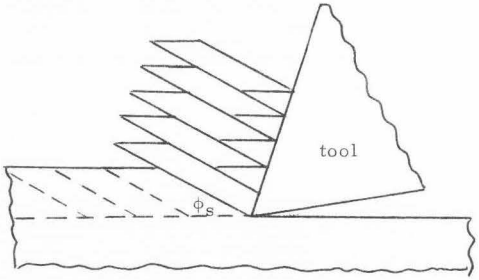

Schematic illustration of chip formation.

(b)

Figure 9. Chip formation in machining.

BURR FORMATION AND PROPERTIES IN SPECIFIC OPERATIONS

Turning operations

There are three basic operations in turning that produce burrs. They are turning, facing, and plunging. (Figure 10) Any of the four types of burrs described earlier can be produced in these operations. The following paragraphs illustrate where these burrs form and how tool geometry affects burr properties.

The typical turning burr shown in Figure 11a is a Poisson Burr. It forms as a result of the effective cutting radius of the tool or as a result of friction on the flank surface. The flank surface is indicated by the angle α. Figure 11b demonstrates the formation of a Roll-Over Burr as the tool passes over an undercut. Figure 11c illustrates the effect of side cutting edge angle (SCEA) on the shape of the potential Roll-Over Burr.

In a typical facing operation a tool with zero or negative SCEA is required to produce a 90° shoulder. The facing tool shown in Figure 12a is fed axially along the part then fed radially out to form the shoulder. As a result of zero SCEA only the Poisson Burr formed in turning occurs at the edge of the part. When a negative SCEA is used (Figure 12b) a Roll-Over Burr forms.

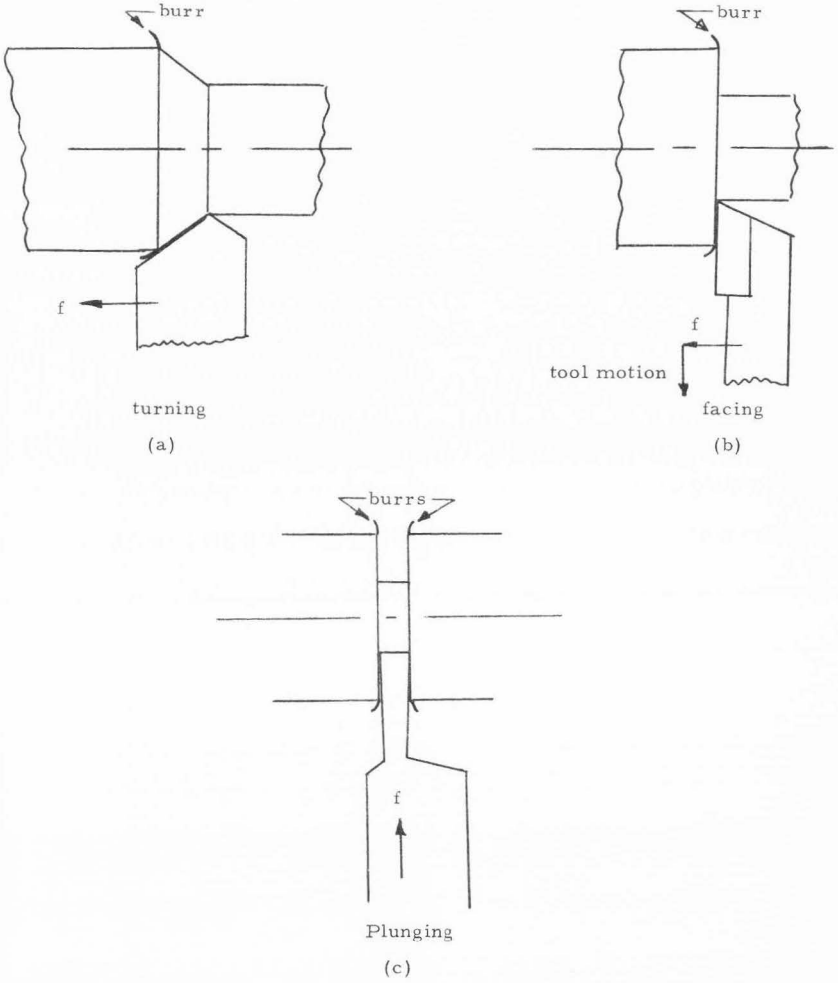

Figure 10. Burrs formed in the basic turning operations.

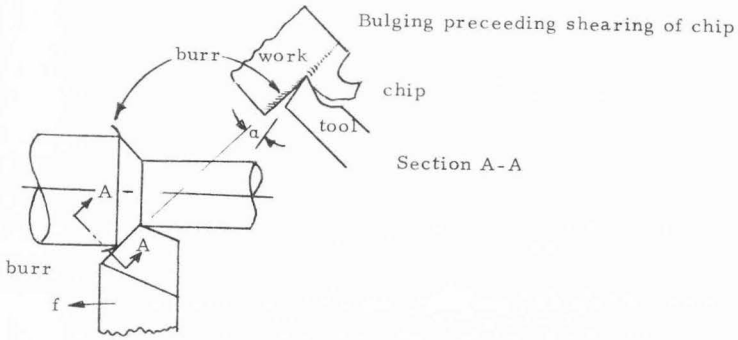

Poisson Turning Burr
(Burr shown is the burr seen if tool is retracted before reaching end of part)
(a)

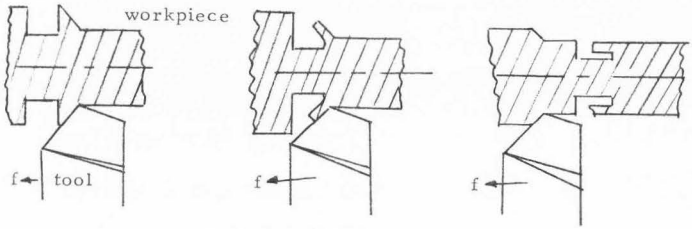

End of cut turning burr
(b)

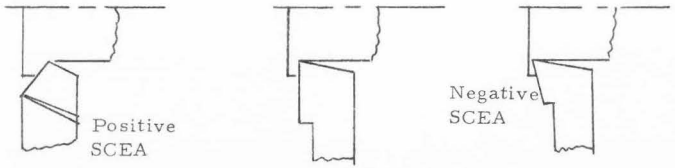

Effect of SCEA on initial burr geometry
(c)

Figure 11. Burrs produced in turning.

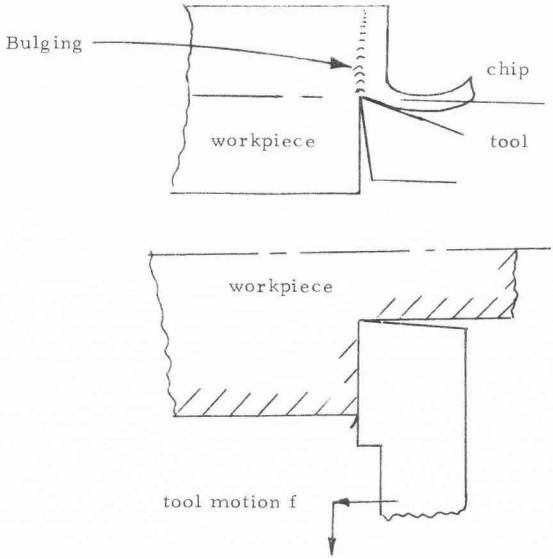

Poisson facing burr (tool has 0° SCEA)

(a)

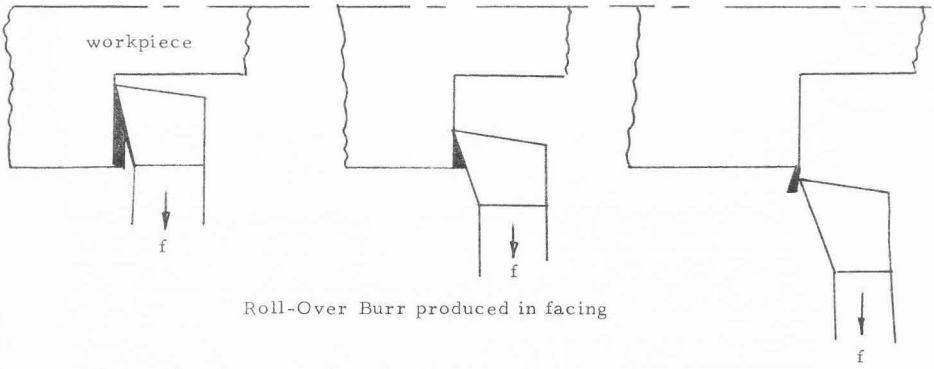

Roll-Over Burr produced in facing

Figure 12. Burrs produced in facing.

When the width of a plunge tool is less than the width of the workpiece (Figure 13) a tear type burr is produced. Once the initial burr forms it does not increase in size as the tool is fed deeper. If, however, high frictional forces occur at the sides of the tool it is possible to force material out the sides of the groove and thus form a Poisson Burr. Such a burr should be thicker than the normal tear burr. If the tool is a cut off tool, as it nears the center of the workpiece the high thrust forces will bend the thin cylinder of the material holding the workpiece to the bar stock. (Figure 13) Shortly after bending begins the part will fracture and fall free of the bar stock. The small cylinder of material remaining on the workpiece is the cut-off burr.

When the width of the plunge tool is wider than the length of the portion being machined, the condition shown in Figure 3 exists and Poisson Burrs occur at the sides of the workpiece.

To determine the effects of SCEA, radial depth of cut, feedrate, and rake angle on Poisson turning burrs, 53 specimen were machined and measured. The workpiece material was 1/2 inch diameter 303Se stainless steel in the cold drawn condition. Table 1 lists the range of variables studied. Appendix Table B1 lists the parameters and results for each specimen. Carbide inserts were used on all cuts. With the exception of rake angles all variables were tried at all combinations shown. Using analysis of variance techniques it was determined that

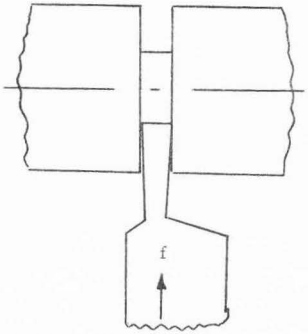

Illustration of plunge cut
(a)

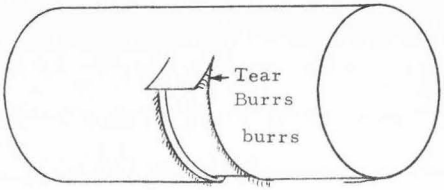

Plunge cut Tear Burrs
(b)

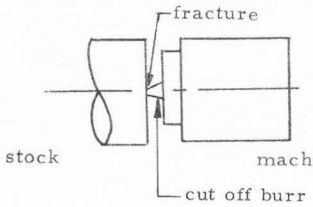

Definition of cut off burr
(c)

Figure 13. Burrs produced by plunge cutting.

Table 1. Variables studied in turning tests

SCEA	Depth of cut (inch)	Feedrate (1 pr)	Rake angles
$17\ 1/2^{o}$	0.040	0.0021	15^{o}
0^{o}	0.070	0.0032	5^{o}
$-17\ 1/2^{o}$	0.100	0.0043	-4.3^{o}
		0.0065	

SCEA, depth of cut, and feedrate all significantly affected the length of burrs produced. As noted in Appendix Table C1 all interactions between these variables were also significant. As shown in Appendix Table B1 and the following graphs the impact of these variables was obvious even without a computer analysis.

The tremendous influence of SCEA on burr length and thickness appears to be the result of a BUE and high strain hardening. Negative SCEA are frequently used in precision finishing operations but burr sizes do not approach those observed in this study. Three factors appear responsible for this anomality.

A) Workpiece vibration allowed the tool to rub the workpiece before entering the cut.

B) A built up edge occured when using 0 and $-17\ 1/2^{o}$ SCEA.

C) The chip breaker groove was filled by BUE material at 0 and $-17\ 1/2^{o}$ SCEA.

Essentially it appears that the slenderness of the workpiece allowed the cutting tool to skip in and out of the cut and consequently producing a great deal of rubbing. This rubbing work hardened the surface which increased cutting difficulty. Rather than shear as in normal cutting it was easier for material at the edge to flow out laterally. The fact that no coolant was used and that the tool kept the chip near the workpiece rather than moving it away from the workpiece accentuated the problem. In some instances red hot chips were produced. In this situation the material would be very gummy which further restricts free cutting. As material welded in the chip breaker groove a negative rake tool was effectively produced which further restricted flow.

It would appear that these conditions could be prevented by using flood coolant and feedrates better matched to workpiece stifness. Eliminating the chip breaker groove should also help produce easier cutting.

The assumptions made in deriving the Poisson Burr equations appear to be satisfied from the data presented in Figures 14-16. The assumption that cutting pressure is independent of feedrate and speed is largely justified although some feedrate effect is noticeable. If ϕ_a in [1] is -60° then the predicted burr thickness would be 0.4 times the effective cutting radius. A cemented carbide tool could easily have a cutting edge radius of 0.0020 inch which would predict a 0.0008 inch thick burr. As noted in Figure 16, a typical burr thickness

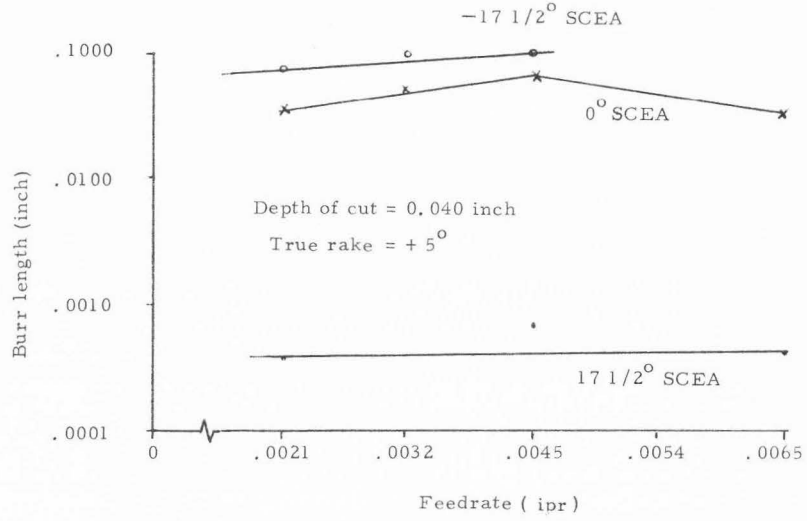

Figure 14. Effect of feedrate and SCEA on burr length. (Poisson Burr in a turning operation)

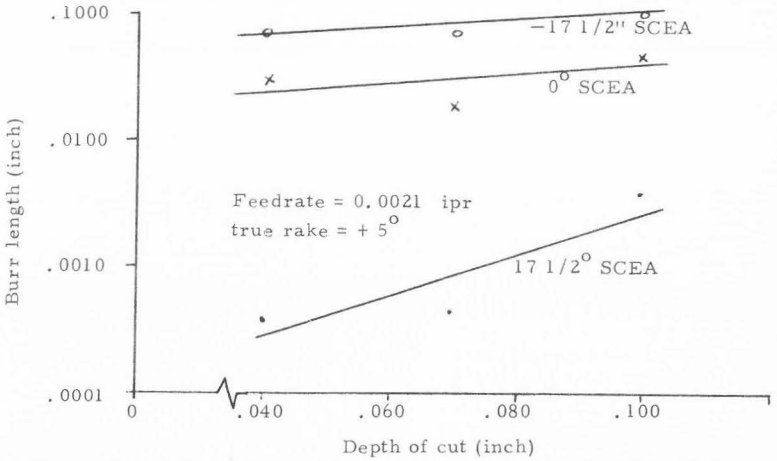

Figure 15. Effect of depth of cut and SCEA on burr length. (Poisson Burr in a turning operation)

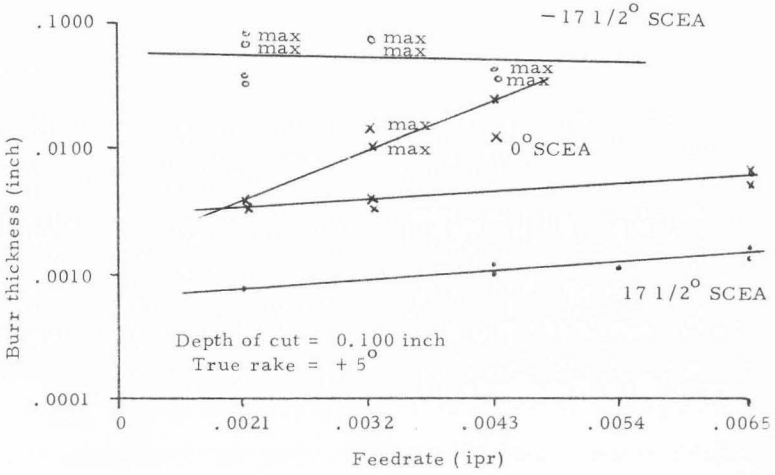

Figure 16. Effect of feedrate and SCEA on burr thickness. (Poisson Burr in a turning operation)

would be 0.0010 inch. Thus the theory can predict burr thickness closely.

As shown in Figure 15 burr length is proportional to the depth of cut. This agrees with the theory [3]. Again assuming $\phi_a = -60^o$ and that $\nu = .3$, $E = 30 \times 10^6$, and that σ_a (which is the yield stress of an equivalent perfectly plastic material) is 160,000 psi the following burr length is predicted,

$$\Delta h \approx \frac{h}{2} \left[- \frac{\sin \phi}{\sqrt{3} \cos \phi + \sin \phi} \right] \qquad [12]$$

For ϕ = small negative angles (0^o -30^o for example) Δh ranges from 0 to $\frac{h}{1.4}$ thus the length predictions are in the correct order of magnitudes provided ϕ is a small negative angle.

At this point it is significant to note that in most turning operations the tool is allowed to dwell at a shoulder before it is retracted. Although this is required to produce an even shoulder it is not hard to envision that this dwell could influence the burr size. The influence could be the result of rubbing or the fact that in the first revolution of the workpiece after the feed is stopped the tool is making a clean up cut. This clean up cut varies in thickness from zero to whatever the feed was per revolution. For materials sensitive to feedrate this could produce a burr which varies around the diameter of the part. This effect has been noted on some materials.

In these tests and in other work on 304 stainless steel and 1020

cold rolled steel, it has been observed that the length of the very large burrs is proportional to the axial length of cut. This apparently is due to the fact that it is easier for the material to push out the sides of the workpiece than to shear. To maintain conservation of mass, if the material does not shear and the tool continues to advance, the material must squirt out the side. This effect is similar to squeezing a tube of toothpaste. The more the tube is compressed, the longer the ribbon of toothpaste becomes. The burr eventually is forced out radially far enough that the tangential stresses on the burr create radial cracks. The resulting workpiece then looks like a daisy (the burr being similar to the petals of the daisy). In some cases the radial cracking begins earlier and the burr looks similar to a hundred pieces of yarn projecting from the workpiece. This dependancy on length of cut does not occur on what is considered a normal burr.

Rake angle effects were studied in one brief test. As shown in Figure 17 and 18 there was little difference produced by the + 5 and + 15 degree rake angles. The −4.3 rake which was obtained by turning the carbide insert upside down in its holder produced burrs three times larger than those produced by positive rakes. At + 17 1/2 SCEA the burr produced by the negative rake tool was 0.002 thick compared with 0.0012 thick for the + 15° rake tool. It would appear that negative rake angles produce thicker and longer burrs.

A brief test of Roll Over Burrs formed in turning indicates

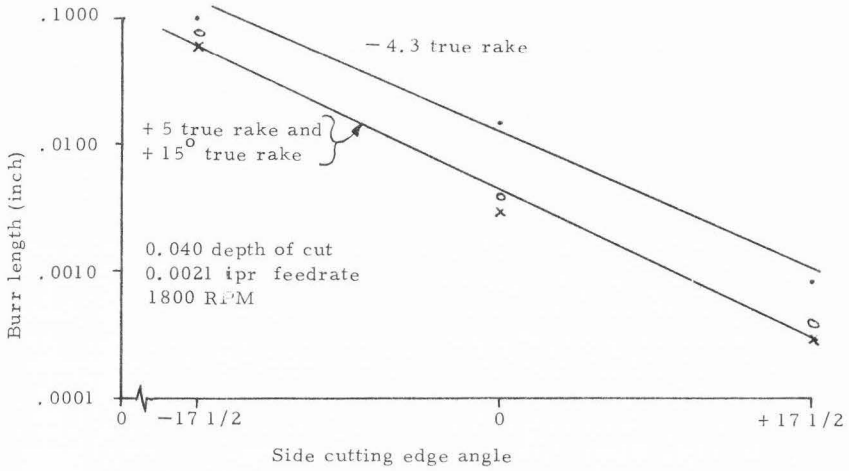

Figure 17. Effect of SCEA and true rake on burr length. (Poisson Burr in a turning operation)

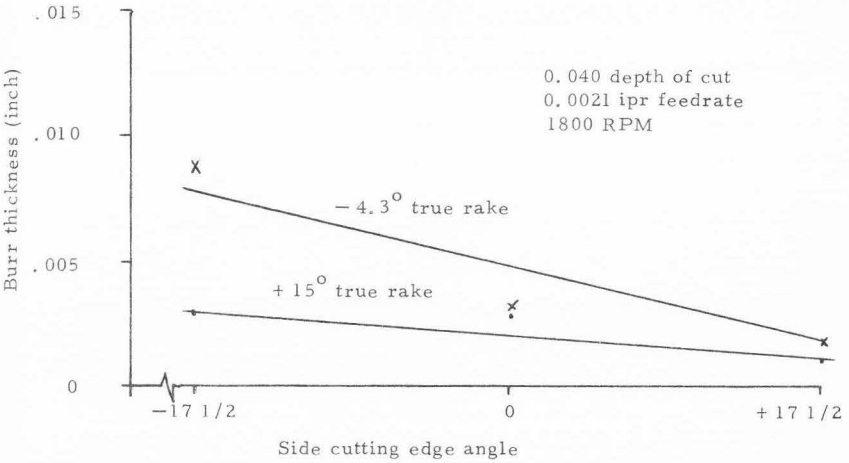

Figure 18. Effect of SCEA and true rake on burr thickness. (Poisson Burr in a turning operation)

that a 0 zero degree SCEA produces thicker burrs than does a 17 1/2 degree SCEA tool. (Figure 20) The effect of depth of cut on this type of burr appears unusually large. Since Figures 19 and 20 are based on only seven specimen the results can only be treated as preliminary trends. When the tool attempted to bend the material over into the undercut shown in Figure 11b most of the material broke free, before it was completely bent over. The result was a short burr on the workpiece and a loose ring of material encircling the workpiece.

Using a breakaway tool holder eleven plunge cuts were made with a tool which was wider than the area being machined. At 0.002 ipr feed, 425 rpm, 20^{o} back rake, 0^{o} side rake and 8^{o} end relief, the Poisson Burr appeared to be formed by the flank surface. Examination of the remaining ten specimen provided no conclusive evidence to indicate at what po nt the cylindrical mode begins and the flank pressure mode of formation ends.

Milling operations

Milling operations such as side milling, end milling, and face milling can also produce each of the four basic types of burrs. In a typical slotting operat ion involving a side milling cutter and through slots, burrs are produced on eight different edges. (Figure 21) If the cutter has a helix angle, each of the burrs will have different properties. This is a highly significant observation for anyone involved in precision burr removal--in a single operation without changing any variable,

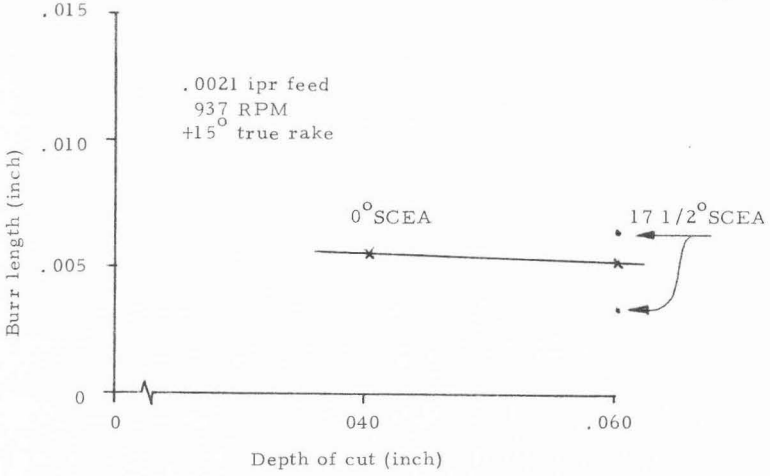

Figure 19. Effect of depth of cut and SCEA on burr length. (Roll-Over Burr in a turning operation)

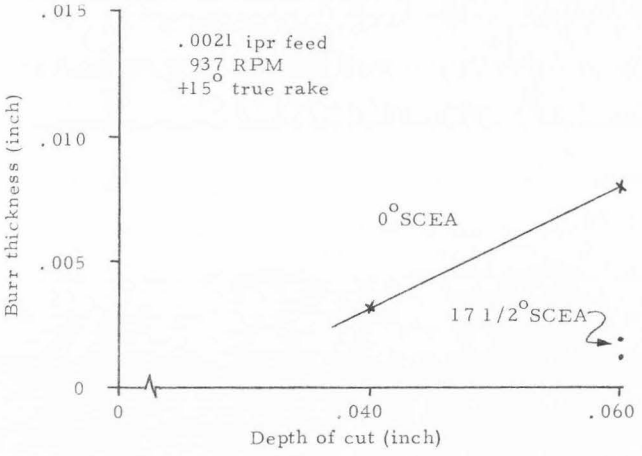

Figure 20. Effect of depth of cut and SCEA on burr thickness. (Roll-Over Burr in a turning operation)

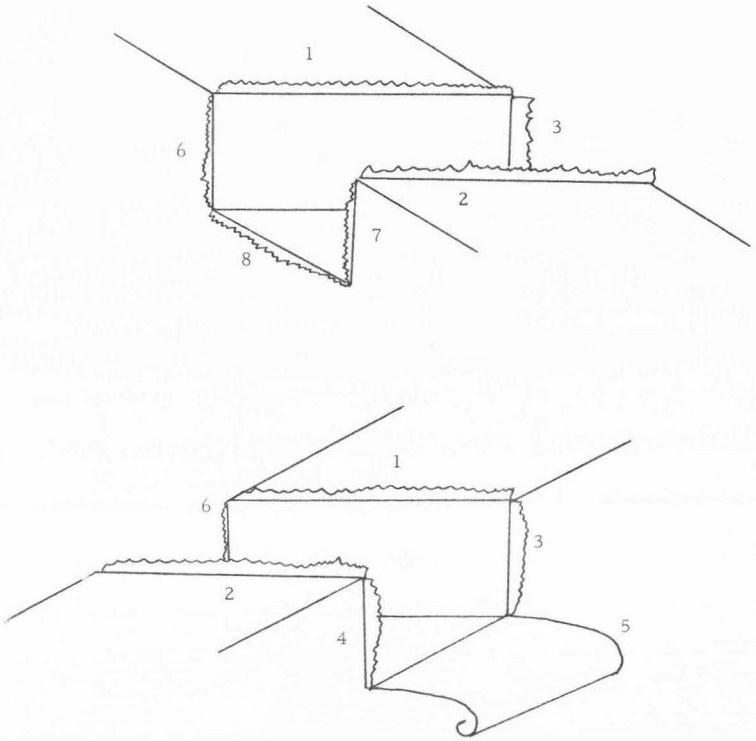

Figure 21. Burrs produced in side milling.

eight different burrs with widely varying properties can form.

From Figures 22 and 23 it can be seen that burrs No. 1 and No. 2 in Figure 21 are produced as the cutter tears the chip from the top surface. These burrs therefore are tear type burrs. Burr No. 8 is the entrance burr. Burrs No. 6 and No. 7 can be either entrance burrs or tear type burrs. In either case they are formed by several teeth rather than an individual tooth. This is more readily seen in Figure 22a. As the tool progresses forward each succeeding tooth enters the workpiece a little lower than the previous tooth. Burrs No. 3 and 4 are also tear type burrs like No. 1 and No. 2. Burr No. 5 is the Roll Over Burr. Figure 23b illustrates the periodic nature of burrs No. 1 and No. 2.

Figure 24 illustrates one significant difference between milling and most other conventional progresses. The chip thickness varies throughout the cut. Points 2x, 2y, and 3y illustrate that the closer the cutter comes to the end of the part the smaller the depth of cut becomes. In addition the closer the tool gets to the edge the more horizontal the cutting force becomes. Although the path of the teeth can be calculated readily from Martellotti's equations (23) the depth of cut taken by the final tooth cannot be calculated precisely unless the exact location of some tooth is known relative to the exit edge of the workpiece. In production such a relationship between a cutter tooth and the workpiece edge is entirely random.

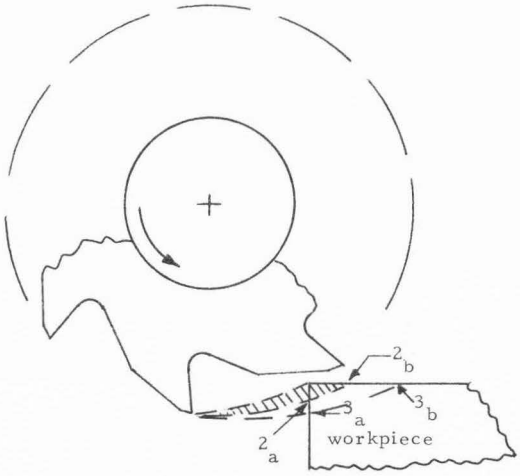

Figure 22. Milling cutter path and chip size
(a)

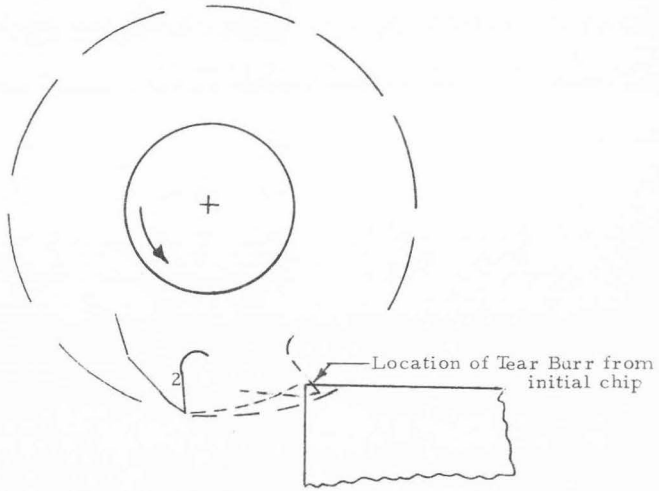

Figure 22. Tooth exiting from workpiece
(b)

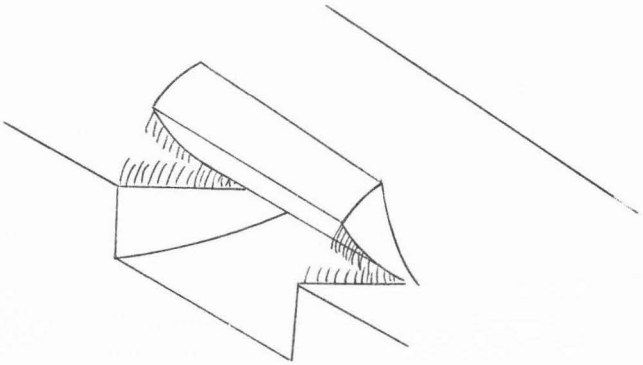

Separation of initial chip
(a)

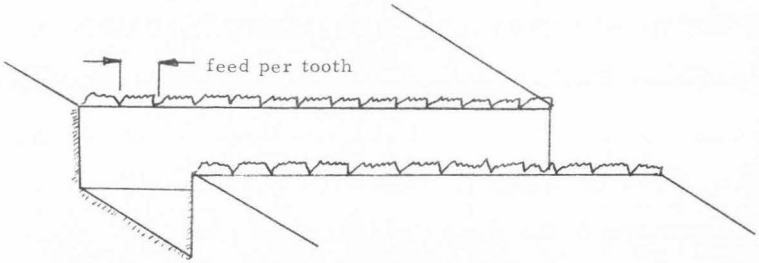

Periodic nature of milling burr
(b)

Figure 23. Chip separation and tear type burr in milling.

Burrs produced in climb milling can differ significantly from those produced in conventional milling. The first obvious difference is that the Roll-Over Burr occurs on the entrance side of the cutter. (Figures 25 and 26) Similarly, in forming the last chip the tooth generates what has previously been called the entrance Poisson Burr. With some thought it is also obvious that a Tear Burr still occurs on the top surface but much different tooth approach angles are involved.

The helix angle (axial rake) on a side milling cutter will significantly affect the properties of the burrs produced. From Figure 27 it is easy to see that the tooth corners on the a_1 side of the cutter will exit from the cut before those on the a_2 side. As a result burrs on the a_1 side tend to be sheared more than torn. From the geometry on the a_2 side it is easy to see that there is more of a tendancy to roll the burr over. A cutter without a helix angle exerts equal forces on both sides of a tooth. Using a zero helix tool, burrs produced by the right side of the cutter will be identical to those produced by the left side. Tools having a helix angle will produce longer and more highly strained burrs on the trailing tooth edge than on the leading edge.

To determine the quantitative effects of helix angle, depth of cut and feedrate on side milling burrs, tests were performed using eight machining combinations. The workpiece material was 303Se stainless steel. Table 2 indicates the combination studied. The

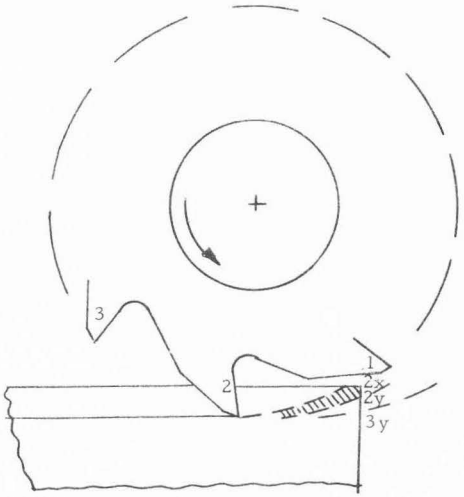

(a)

Figure 24. Cutter exiting from workpiece.

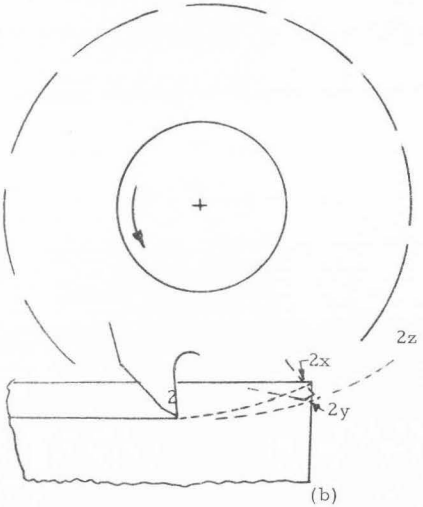

(b)

Figure 24. Tooth position at cutter exit.

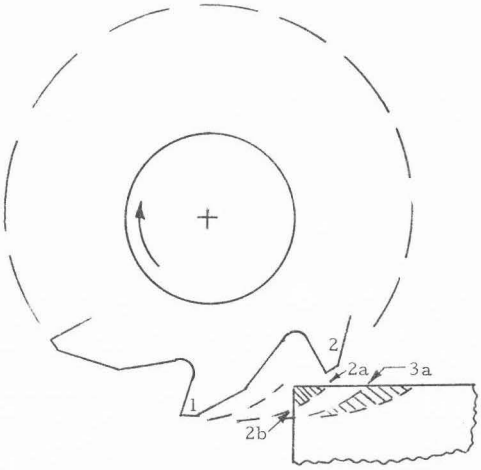

Tooth path in climb milling (entrance side)
(a)

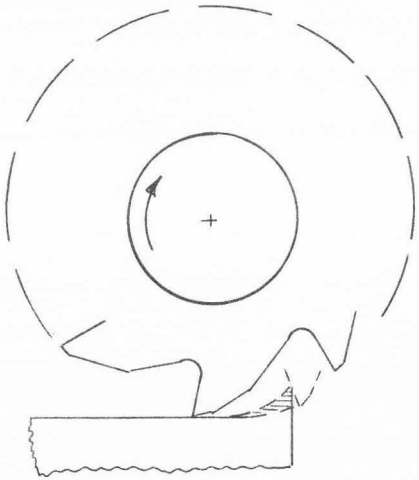

Tooth path in climb milling (exit side)
(b)

Figure 25. Path generated by a plain milling cutter in climb milling.

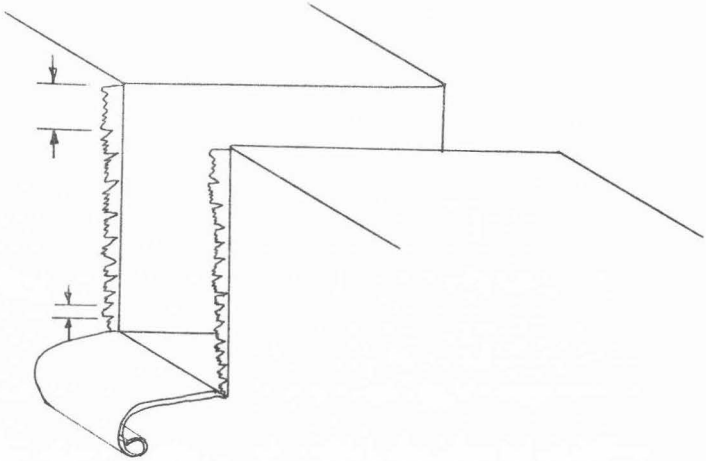

Figure 26. Illustration of climb cut entrance burr.

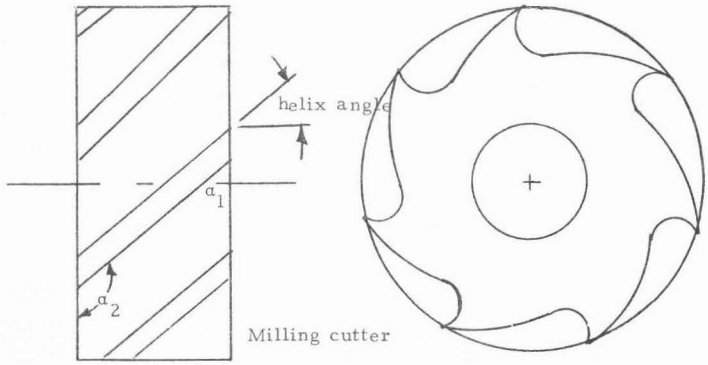

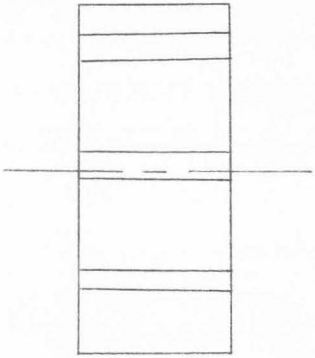

Figure 27. Edge angles resulting from a helix angle.

length of burrs at the eight locations indicated in Figure 21 was measured. The resulting measurements are presented in Appendix Table B5.

Table 2. Side milling test conditions*

SEϕ No.	Helix Angle (Degrees)	Depth of cut (inch)	Feed (IPR/T)	Feedrate (IPM)
1	0	0.125	0.002	3.5
2	0	0.125	0.00057	1.0
3	0	0.375	0.002	3.5
4	0	0.375	0.00057	1.0
5	10	0.375	0.002	3.5
6	10	0.375	0.00057	1.0
7	10	0.125	0.002	3.5
8	10	0.125	0.00057	1.0

*Using 4" diameter 1/2" wide side milling cutters with 18 teeth at 98 RPM. The cutter with 10^{o} helix is a staggered tooth cutter.

An analysis of variance (ANOVA) was performed for each burr. The ANOVA for these burrs is presented in Appendix Tables C8-C14. The results are summarized in the following table. As seen in Table 3, burr No. 1 was influenced by the helix angle, but not by depth of cut or feedrate. Burr No. 2 however was influenced by depth of cut and feedrate but not helix angle.

Table 3. ANOVA results for side milling (Burr length data)

Code	Source of Variation	Variance Ratio Burr Location No.							
		1	2	3	4	5	6	7	8
A	Helix Angle	5.62	----	----	10.6*	9.2*	----	5.0*	12.1*
B	Depth of cut	3.05	5.62*	2.98	----	----	----	----	10.4*
C	Feedrate	----	5.62*	----	----	3.62	10.0*	4.18*	6.0*
AB	Interaction	----	----	----	----	----	----	----	14.0*
AC	Interaction	----	----	----	----	----	----	5.0*	43.3*
BC	Interaction	----	----	----	----	----	----	----	18.2*
ABC	Interaction	----	----	5.5*	2.83	2.32	----	5.9*	34.0*
	Error MS	.43	.91	17.31	8.76	9747.0	.06	.04	.025

* indicates significance at the .05 level

Helix angle does affect burr length. Intuitively one would have expected burrs No. 3 and No. 4 to exhibit trends similar to burrs No. 1 and No. 2. Statistically they did not however. The following graphs illustrate the significant trends for each of the burrs. Table 4 provides data on the relative sizes of the burrs produced. In analyzing the effect of heliz angle it is important to observe that a staggered tooth cutter was used as the 10^{o} helix tool. Thus no burr was produced by a trailing edge.

Table 4. Typical lengths of side milling burrs

	Burr location No.							
	1	2	3	4	5	6	7	8
Length	.0028	.0020	.0140	.0073	.0600	.0001	.0004	.0002

In reviewing the data as a whole the following items appear most significant:

A) Depth of cut did not greatly influence burr length. When the depth of cut approaches the cutter radius depth probably would be significant.

B) The helix angle does appear to have some impact on burr length.

C) Feedrate effects appear to be fairly small.

As shown in Table 4. the entrance burrs (No. 6, 7 and 8) are very small as predicted by Figure 4 for 303Se stainless steel. The exit Tear Burrs (No. 3 and 4) are noticeably larger than the top Tear Burrs (No. 1 and 2). The length of burr No. 5 is proportional to the depth of cut. As noted elsewhere in this report burr No. 5 is brittle and tends to break off easily.

The length of burrs No. 1 and No. 2 correspond to the lengths predicted in Appendix A for Tear Burrs. Burrs No. 3 and No. 4 are noticeably longer than predicted. The length of burr No. 5 agrees with the predictions in Appendix A. Although no thickness measurements were made on the burrs produced by the side milling cutters

data is available from one of the author's earlier reports (15). In that report it is noted that burr thickness was largely independent of feedrate. Using a 25^{o} helix cutter the following comparisons were made. (See Figure 28)

Table 5. Relative burr thickness of side milling burrs[a]

	Burr Location[b]			
	6	7	3	4
Climb cut	.0015	.0001	.0015	.0005
Conventional cut	.0002	-0-	.0025	.0010

b) Locations 7 and 4 correspond to the leading edge of the cutter teeth; locations 6 and 3 correspond to the trailing edge.

a) From Gillespie (15).

The hardness of the burrs reported in (15) follow the general trend predicted by [11]. Hardness values ranged from a Brinell 372 to Brinell 600 for an initial hardness of Brinell 276. The maximum theoretical hardness possible in 303Se stainless steel is in the order of Brinell 500.

A typical thickness of the Roll Over Burr in the current study was .002. By extrapolating Shaw's force data (37) and assuming a strain hardening exponent of .34, $\sigma_o = 205,000$, $\epsilon_f = 1.16$, $b = 3/8$, $t = .001$, $\Theta = 105^{o}$, the predicted burr thickness (from [A36]) is .0066. Although the predicted thickness is a factor of 3 larger than

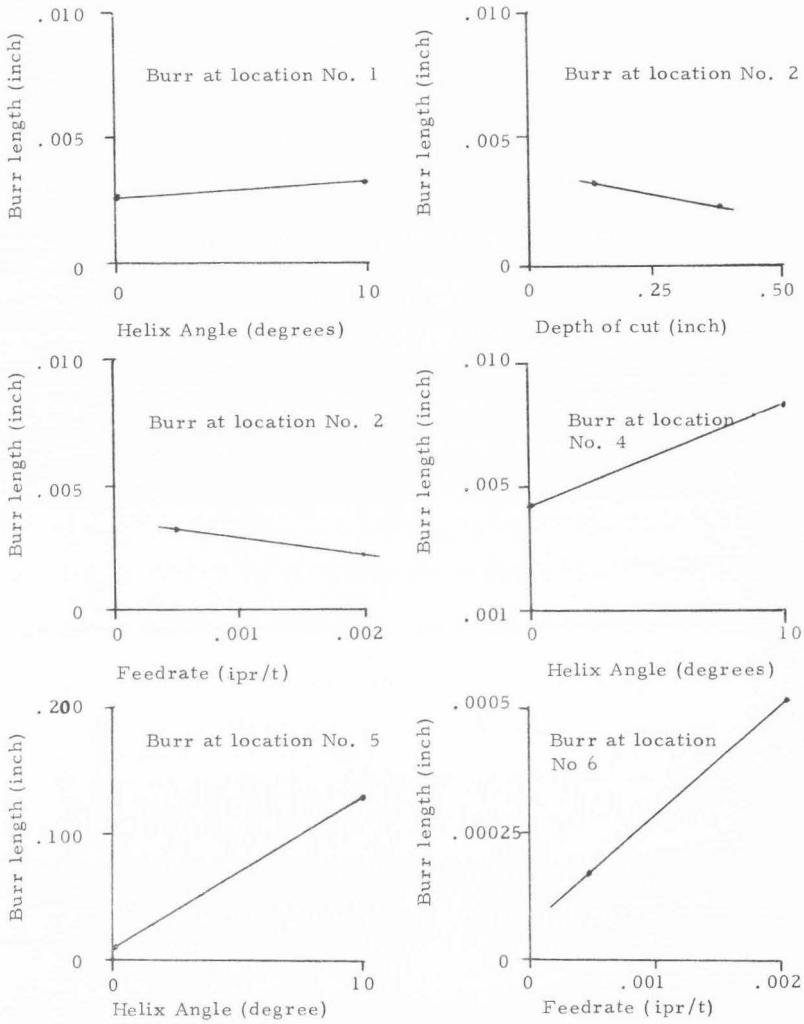

Figure 28. Effects of machining conditions on side milling burrs.

the measured size it is still a reasonable estimation of the maximum possible burr thickness. If one were to assume that redundant work in bending consumed twice the ideal work then the prediction would agree with the experimental data. As discussed in Appendix A it is not unreasonable to make such an assumption about redundant work.

End milling, like side milling produces several burrs in a single cut. In a profiling operation such as shown in Figure 29, six different burrs are produced. Because the cutting process is significantly different from side milling the burrs at any particular location will not have the same properties that a burr produced by a side mill have.

Two aspects of end milling warrent particular comment. The burr produced by the bottom of the end mill (burr No. 9) will vary considerably with the cutter used. The geometry of end mill end's varies greatly from one manufactured to another. The fact that the entire bottom of the cutter is in physical contact with the burr increases the probability of high work hardening. One unique aspect of end milling is that when the tool is making a full diameter cut, one side is making a conventional cut while the other is climb milling. For the rotation and feed direction shown in Figure 29 the left side is cutting conventionally, while the right side is climb cutting. Thus burr 6 in Figure 30 is an entrance type burr while burr 7 is an exit type burr.

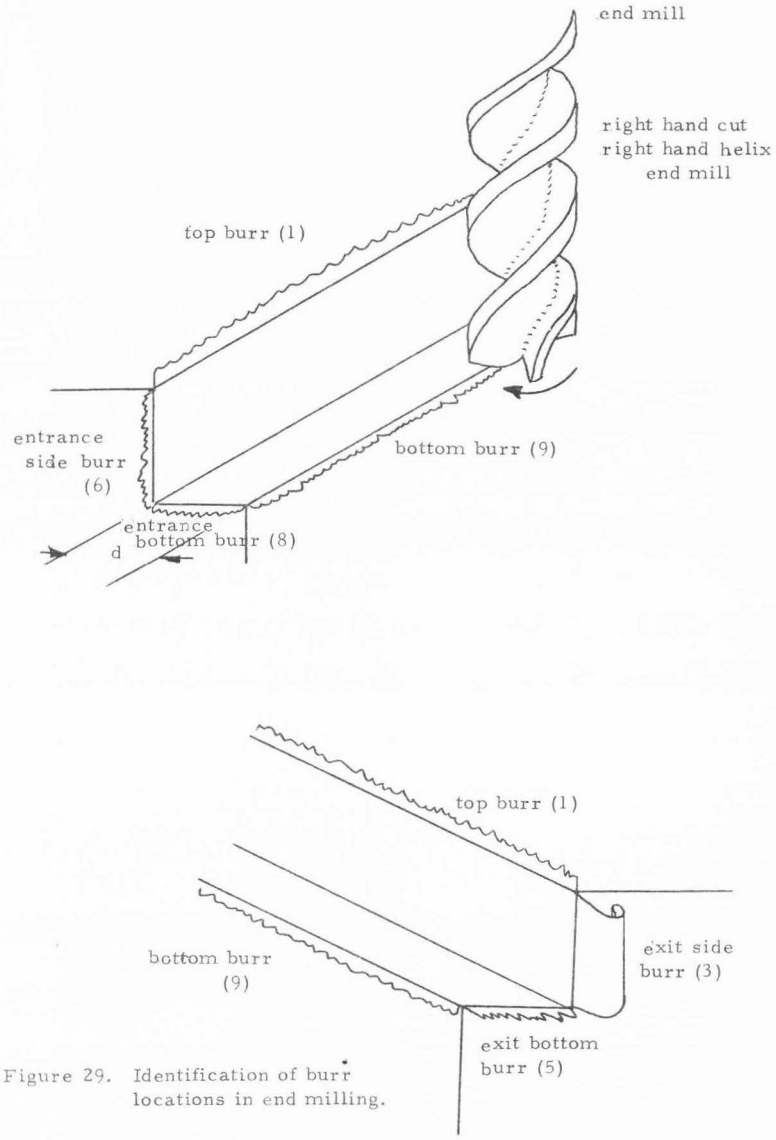

Figure 29. Identification of burr locations in end milling.

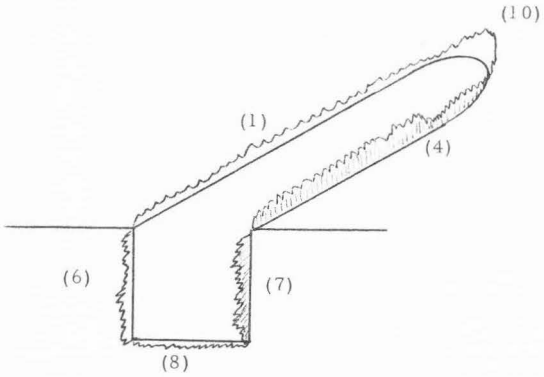

Blind channel

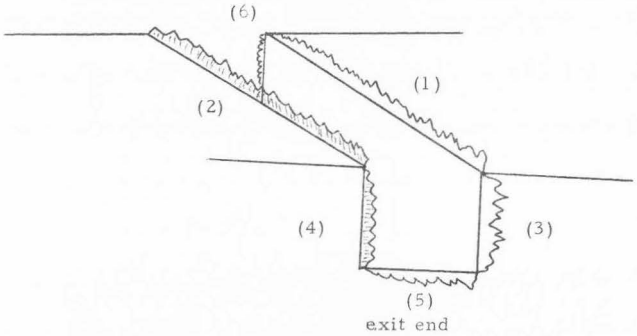

Through s'ot

Figure 30. Identification of burr locations in end milling.

Burr No. 10 represents a transition phase which may or may not be the same as burrs 1 and 2. Burrs 1, 2, 8, 5 and 9 will illustrate a periodicy as a result of the tool feedrate. Figure 31 illustrates how radial depth of cut affects the length of the Roll Over Burr.

Burrs produced by 36 machining combinations were measured to determine the effects of tool diameter, radial depth of cut and feedrate. Table 6 indicates the ranges of each variable studied. Test details and measurements are presented in Appendix Tables B2-B4. Due to tool breakage not all combinations shown were tested. The workpiece material was 303Se stainless steel in the cold drawn condition.

Table 6. End milling conditions studied

Tool Dia	Radial Depth	Feedrate
1/8	.1 DIA	.0005
1/4	.35 DIA	.0020
3/8	.60 DIA	.0035
	1.00 DIA	

As shown in Table 7, end mill diameter and the radial depth of cut significantly influenced burr lengths. Feedrate also influenced most burrs but its influence was smaller than the other two variables. The strong influence of diameter and radial depth of cut on burr 3 is obvious from Figure 31. Significant combinations of variables are

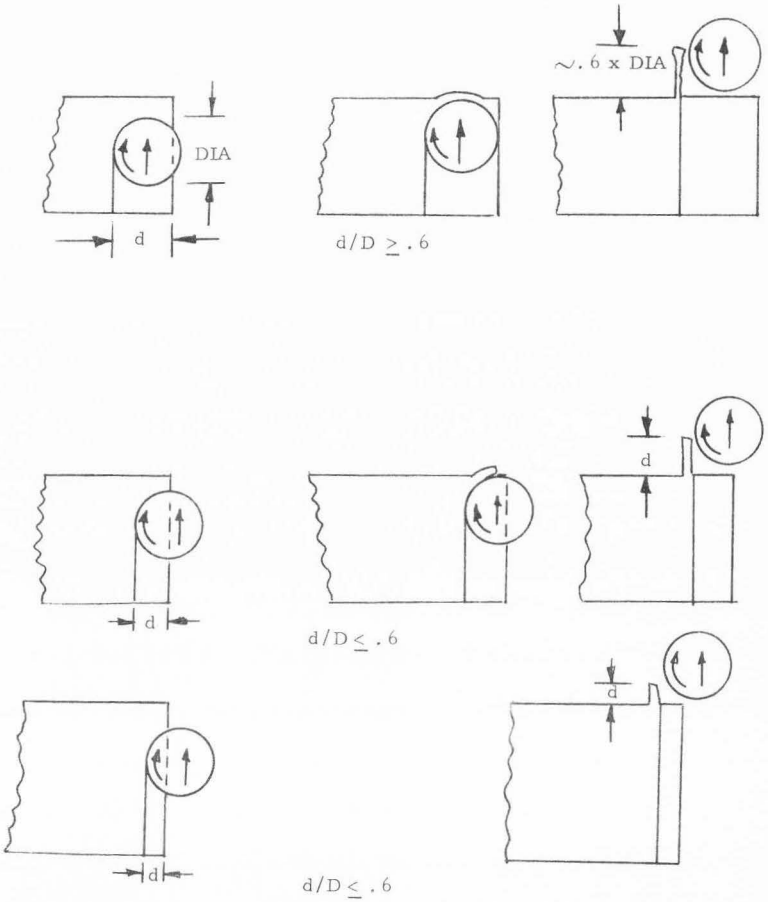

Figure 31. Effect of radial depth of cut on Roll-Over Burr.

plotted for each burr in Figures 32 - 34. Representative lengths of the end milling burrs are shown in Table 8.

Table 7. ANOVA results for end milling (burr length data)

Code	Source of Variation	Variance Ratio Burr Location					
		1	3	5	6	8	9
A	Diameter	59.8*	1,390*	28.2*	4.82*	----	26.8*
B	Depth	78.6*	4,490*	----	----	8.74*	12.4*
C	Feed	44.2*	123*	----	----	----	12.0*
AB	Interaction	21.3*	620*	----	11.0*	----	----
AC	Interaction	21.7*	120*	----	6.35*	----	----
BC	Interaction	21.7*	104*	----	6.68*	----	6.78*
ABC	Interaction	7.75*	68*	----	4.27*	----	4.59*
	Error MS	.091	22	35	.005	.084	.51

* indicates significance at .05 level.

Table 8. Typical properties of end milling burrs

	Burr Location									
	1	2	3	4	5	6	7	8	9	10
Length	.001	.003	.085	.0001	.0024	.0002	.060	.0007	.0029	.0020
Thickness	.0005		.0020						.0020	
Hardness[a]	332								332	

[a] Brinell hardness (original hardness of material was 325)

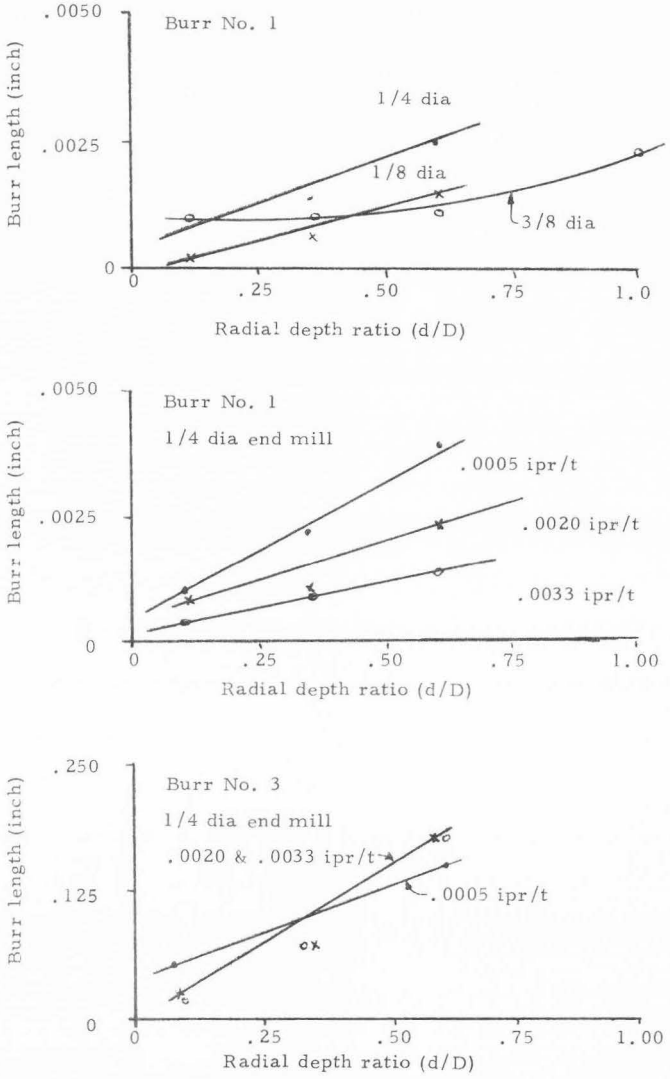

Figure 32. Effects of machining conditions on end milling burrs.

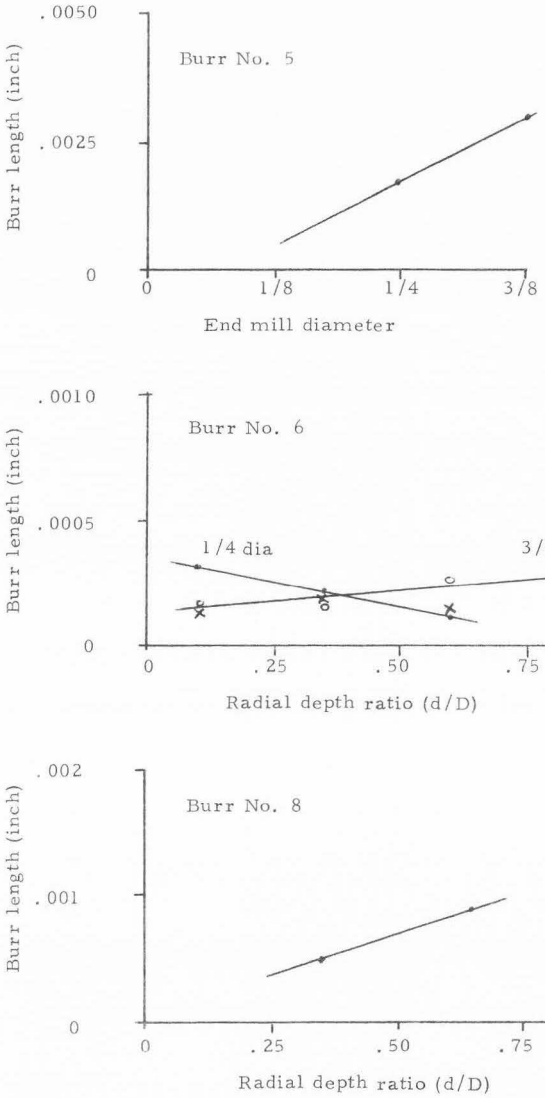

Figure 33. Effects of machining conditions on end milling burrs.

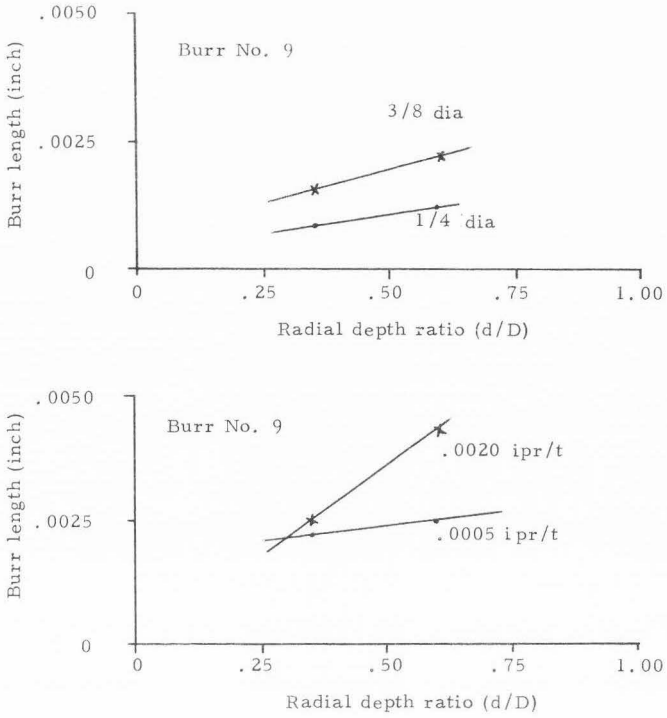

Figure 34. Effects of machining conditions on end milling burrs.

These burr sizes are in line with the previous explanations. Burrs 4, 6 and 8 are entrance burrs. Note however that the right side of burr 8 is in reality an exit burr, thus the average length is greater than burrs 4 and 6. Burrs 1 and 2 are Poisson burrs. It is significant to note that the burr on the climb cut side is longer than the one on the conventional cut side. This has also previously been observed by the author (14). The reason for the difference has not been explained. Burrs 3 and 7 are exit Roll Over Burrs. Burr 9 is one of the larger burrs and is typically thicker than the other burrs. Burr 10 is a transition between burrs 1 and 2 and does have properties between the two.

Only a few measurements of burr thickness were made on the end mill samples. The results agreed with some of the author's earlier findings under similar conditions. The thickness and hardness values shown in Table 8 are from the earlier work (16). In that study it was noted that the helix angle did not influence burr size but it did effect the hardness of burr 9. Feedrate also affected the lengths of burrs 1 and 9.

Grinding operations

Grinding, like all other conventional processes, produces burrs. Burrs are generally small, however, and easily removable. Each grain of abrasive in the grinding wheel acts like the tooth of a milling cutter. Unlike a milling cutter, however, the grain has an effective

rake angle γ of -30° (Figure 35) From the symmetry inherent in the grains it is apparent that the grain also effectively has a -30° lateral rake angle. Thus there is a very strong tendancy to push material laterally. The statistical arrangements of the grains allows some grains to push material toward the center of the part while the next grain will force material off the edge. This random movement of material cuts many burrs or potential burrs free of the workpiece. For this reason a grinding burr will often only be attached to the workpiece for roughly half of its length.

As in milling a small entrance burr is produced when the grinding wheel enters the workpiece. A Roll Over Burr occurs at the point of wheel exit. Figure 36 illustrates burr sizes measured in a brief grinding test of 303Se stainless steel. A standard surface grinder was used with a PA 46-HB-V40 wheel. As shown there the roll over burr (No. 3) was proportional to the depth of cut and the number of passes made. The entrance burr was not dependent on depth of cut or downfeed. Both of these agree with the theory already described. Burrs 1 and 2 are a combination of Poisson and Roll Over Burrs.

The thickness of burr No. 3 is .0005 - .002 inch while burrs No. 1 and No 2 are in the order of .0002 inch thick. Although hardness was not checked by the nature of the grinding operation one can reasonably assume it is near the maximum hardness of the material (about BHN 500 for 303Se stainless steel).

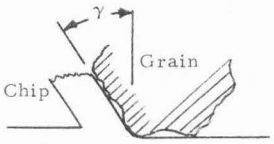

Particle of grain in grinding.
(a)

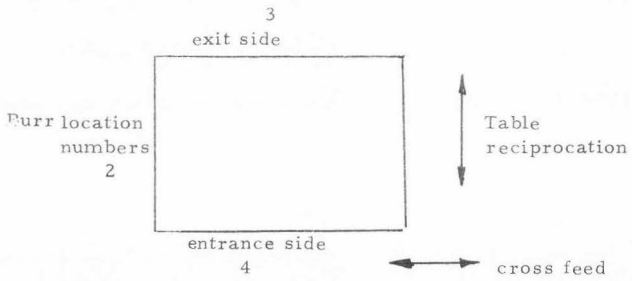

Burr location and specimen placement in grinding
(b)

Figure 35. Effective rake angle and burr location in grinding.

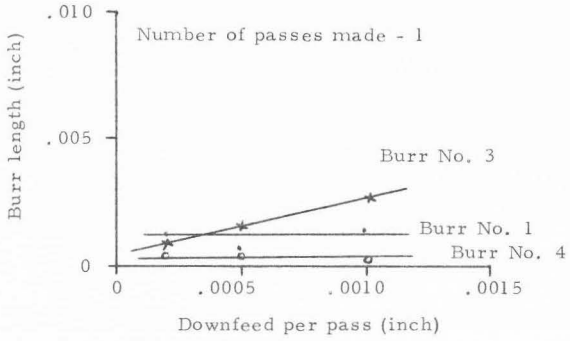

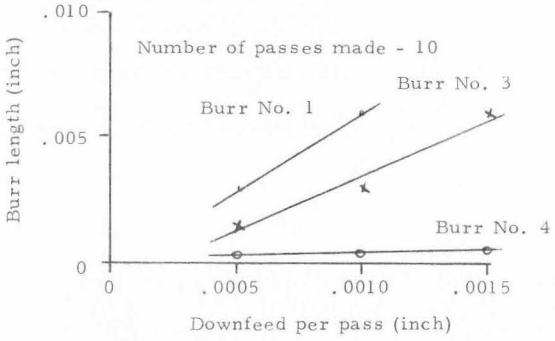

Figure 36. Effects of machining conditions on grinding burrs.

Drilling operations

Burrs produced in drilling occur by three possible models. The burr on the entrance side of the hole is a Tear Burr. A chip begins forming as soon as the cutting lips enter the material, but the burr is not initiated until the 'corners' of the drill begin cutting. As the chip begins moving upward at the corner of the drill it is still attached to the side of the hole. The drill margin forces the chip up and tears it free from the workpiece. Thus a Tear Burr occurs on the workpiece.

In the majority of cases the bottom burr is a Roll Over type burr. As noted by Oxford (28) no cutting can occur at the drill point because there is no rotational velocity at the center of a rotating cylinder. Because of the axial force, drill point acts as a punch. As the drill breaks through the bottom of the workpiece it begins to push material out of its path.(Figure 37) As the point progresses out the bottom the thin flange of material ahead of it begins to tear radially. The drill margins form the burr into a cylinder shape. Because the burr tears radially rather than around the circumference, drilling burrs are usually firmly attached to the hole.

The Poisson Burr can also occur on the bottom side. In this case the drill margin at the corners of the drill have to remove the last vestige of material. (Figure 38) As the margin shears the material it forces material axially down in the same manner as a lathe tool forms a Poisson Burr.

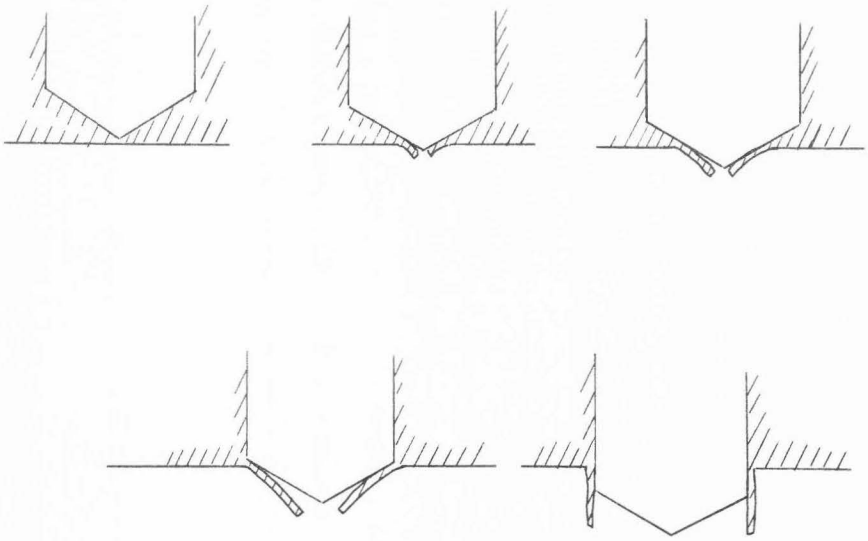

Figure 37. Roll-Over Burr formed in drilling.

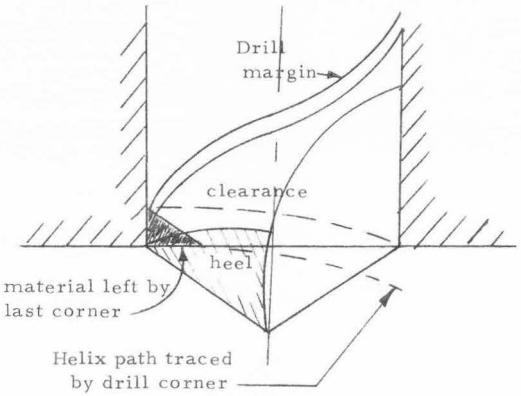

Figure 38. Typical burr formation in drilling.

Table 9 illustrates the drilling combinations studied in one series of tests. Through holes were produced in 1/4" thick 303Se stainless steel in the cold rolled condition. A series of three holes was produced and inspected at each of the conditions shown.

Table 9. Drilling test conditions*

Seq. No.	Helix Angle (Degrees)	Drill Point (Degrees)	Feedrate (IPR)
1	35	118	0.0005
2	35	118	0.0015
3	35	60	0.0005
1	35	60	0.0015
5	25	60	0.0005
6	25	60	0.0015
7	25	118	0.0005
8	25	118	0.0015
9	35	135	0.0005
10	35	135	0.0015

* 1/8 inch diameter solid carbide drill at 1200 RPM.

An analysis of variance indicated that helix angle, drill point angle, and feedrate significantly influenced burr length on both the entrance and exit sides of the hole[a]. Figure 39 illustrates the

[a] The length measurements shown in Appendix Table B7 represent the typical shortest burrs found around the holes. This is felt to be a much more reliable variable than the maximum or average burr length in the case of drilling.

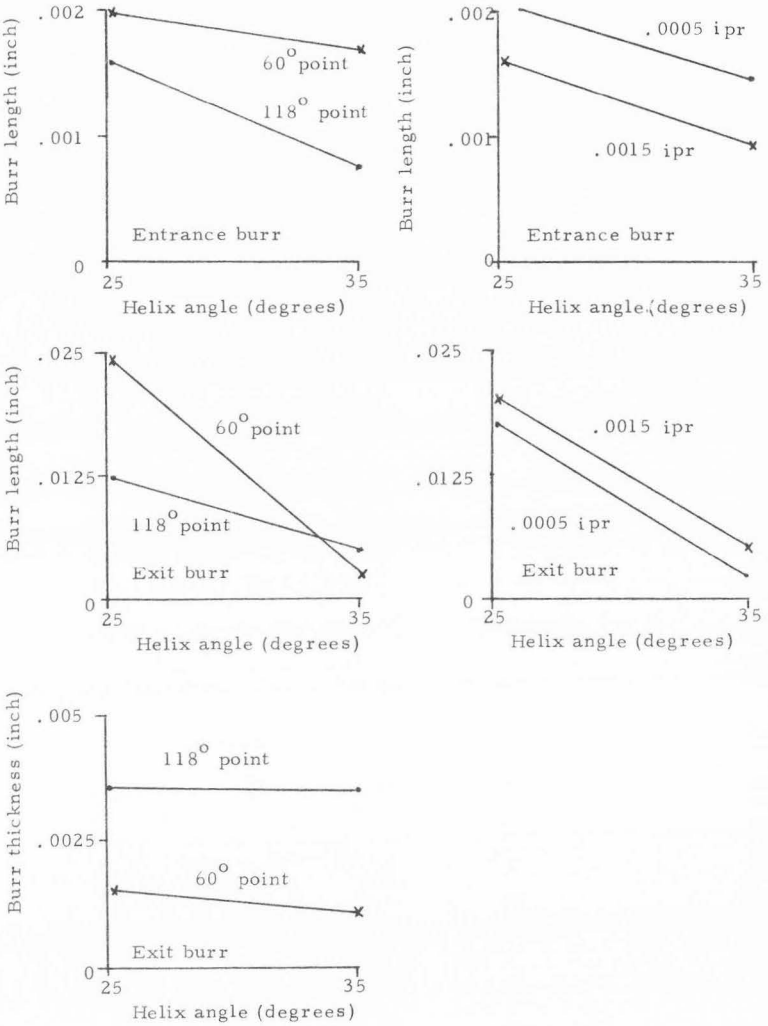

Figure 39. Effect of drilling variables on burr size.

significant trends. The 118^{o} point obviously minimizes the length of burr produced but the 60^{o} point appears to minimize the burr thickness. A high helix angle minimized the burr length but did not significantly affect burr thickness. A higher feedrate increased exit burr length but did nothing to burr thickness. In a preliminary test on effects of drill wear it was observed the initial burrs were longer and thicker than those produced after some wear occured.

In analyzing the burr sizes provided in drilling the primary consideration must be thrust. Any variable which decreases thrust should decrease burr size. A 60^{o} drill point does decrease the thrust as does reducing the feed rate. The apparent success of Haggerty's (17) Spiral Point Drill and the Radial Lip Drill described by Pond (29) and others (2) appears to be a result of lowering thrust or distributing it more uniformly along the cutting edge. There would appear to be a particular corner angle on a drill which minimizes burr sizes. Initial drill wear appears to form the corner to this angle.

GENERAL COMMENTS

Throughout this study burr length has been used as the primary indicator of maching effects on burr formation and properties. In burr removal efforts the more significant variables are burr thickness, volume, and hardness. For any given burr produced in a specific operation the burr properties must be related. Thus through regression analysis thickness, hardness and volume values can be directly related to burr length. For the majority of cases it is reasonable to assume that longer burrs are also thicker than shorter burrs. Such rule of thumb statements, however, are not valid when comparing two different types of burrs.

As seen from the burr measurement data burr sizes may vary considerably along a given cut. Because of this it is necessary to make several measurements to establish a typical size. This becomes exceedingly time consuming when measuring burr thickness and hardness because each burr specimen must be prepared as a metallurigical mount. In any burr study the use of average burr sizes rather than maximum sizes should be used. Wang's study (38) indicates that average burr sizes are 50 times more repeatable than maximum sizes. The use of average sizes does present a problem when burrs have a triangular or curved cross section. The drilling

burrs for example typically demonstrated an exponential shape on the outer surface. It was not uncommon for the burr to be three times thicker at its base than at some point away from the base.

CONCLUSIONS AND RECOMMENDATIONS

Burrs produced in machining operations are formed by three basic mechanisms:

1) Lateral extrusion of material

2) Bending of the chip

3) Tearing of the chip from the workpiece

In the first case machining pressures exceed the yield strength of the workpiece material and produce localized flow at the free edges. The burr produced by this mode of formation has been labeled a Poisson Burr in this report. The Poisson Burr can form by three methods. In the first method the pressure on the effective cutting edge radius produces material bulging all around the cutting edge. In the second method high pressures on the flank surface of the tool produce lateral flow. In the third method the initial indentation of the cutting edge into the workpiece causes material to flow in the direction opposite tool motion. Burrs produced by this latter method are identified as Entrance Burrs in this report.

In the second mechanism of burr formation less energy is required to bend material ahead of the tool than to shear it. As a result the material rolls over out of the path of the tool. This type of burr is labled a Roll-Over Burr in this report.

The third mechanism occurs when the sides of a chip are torn free of the workpiece. The raised material left on the workpiece at this tear is identified as a Tear Burr in this report.

The various means by which each of the burr formation mechanisms occur have been defined for milling, drilling, turning, and grinding operations. The effects of tool geometry, feedrate, and depths of cut has been analyzed for each of these machining operations. Because of the large number of variables studied it is not appropriate to summarize the machining observations here. In end milling alone for example 90 entries would be required to summarize machining effects. Tool wear effects have been analyzed quantatively. With the exception of drilling, toolwear increases burr thickness and length. Initial wear in drilling appears to reduce burr size; subsequent wear will increase burr size.

Analytical techniques for predicting burr properties have been developed. These techniques appear to match experimental findings closely.

On the basis of this study there is no way machining burrs can be prevented. By appropriate selection of machining variables and setup burrs can be kept small. It is also significant that in a single cut 10 different burrs can result. This large variation in burr sizes must inevitably affect precision deburring efforts.

Several areas requiring further investigation are apparent from this study. In recommending such studies the most significant

would be an analysis of the burr formation produced by the flank of the cutting tool. An empirical verification on other materials is needed for the models proposed in this study. The effects of tool wear and cutting velocity also merit analysis.

Ultimately the results of this and the recommended studies must be analyzed from the standpoint of economic trade offs in burr removal. The study of optimum machining conditions as a function of burr removal and machining costs has to be worthy of considerable future study.

BIBLIOGRAPHY

1. American Society of Tool and Manufacturing Engineers. Tool Wear in the Cutting of Thin-Guage Steel Sheets. ASTME Research report, No. 22. May 1, 1959. (Translation and discussion of article by Otto Kienzle and D. Werner Kienzle. Stahl und Eisen. 78(12):820-828. June 12, 1958.

2. Anonymous. Cost-Saving Drill Point Relies on Accurate Grind. Tooling and Production: 81. February 1970.

3. Biegel, John E., and Robert E. Holmes. Development of a Punchability Rating Method for Electrical Steels. ASTME Research Report, No. 30. March 1, 1961.

4. Bridgman, P. W. Studies in Large Plastic Flow and Fracture. McGraw-Hill Book Company, Inc., New York. 1952.

5. Buhler, Hans, and Fedor Pollmar. The Formation of Burrs in the Cutting of Thin Sheet. Bander-Bleche-Rohre. 12(3)105-111. March 1971.

6. Crane, E. V. Plastic Working of Metals and Power Press Operations. John Wiley and Sons, Inc., New York. 1939.

7. Datsko Joseph. Material Properties and Manufacturing Processes. John Wiley & Sons, Inc., New York. 1966.

8. Dugdale, D. S. Wedge Indentation Experiments with Cold Worked Metals. Journal of Mechanics and Physics of Solids. 2:14. 1953.

9. Ford, Hugh. Advanced Mechanics of Materials. John Wiley and Sons, Inc., New York. 1963.

10. Form, G. W. and H. Beglinger. Fundamental Considerations in Mechanical Chip Formation. Annals of the C. I. R. P. 18:153-167. 1970.

11. Foss, F. E. and R. C. Brumfield. Some Measurements of the Shape of Brinell Ball Indentations. Proceedings of the American Society for Testing Materials. Vol. 22, Part 2, pp. 312-334, 1922.

12. Gillespie, L. K. Bendix Technical Quarterly-Mechanical Products Engineering. Bendix Corporation, Kansas City, Missouri. August 1972.

13. Gillespie, L. K. Deburring: A Guide to Process Selection. (unpublished report) Bendix Corporation (Kansas City Division) July 1972.

14. Gillespie. L. K. Precision Deburring of Miniature Parts: Interim Report. (unpublished report) Bendix Corporation (Kansas City Division) April 1972.

15. Gillespie, L. K. Precision Deburring of Miniature Parts: Interim Report. (unpublished report) Bendix Corporation (Kansas City Division) September 1972.

16. Gillespie, L. K. Vibratory Deburring. Bendix Corporation (Kansas City Division) Final Report of EP 6984390 (in preparation) March 1973.

17. Haggerty, W. A. Effect of Point Geometry and Dimensional Symmetry on Drill Performance. International Journal of Machine Tool Design and Research 1: 41. 1961.

18. Hugo, Harding R. How to Improve Metal Stamping Die Performance. Sheet Metal Industries. pp. 120-135. February 1971.

19. Kalpakjian, Serope. Mechanical Processing of Materials. D. Van Nostrand Company, Inc., Princeton, New Jersey, 1967.

20. Kronenberg, Max. Machining Science and Application. Pergamon Press, New York. 1966.

21. Kurrein, Max. Plasticity of Metals. Charles Griffin & Co. Ltd. London. pp. 144-145. 1964.

22. McBride, James Nielson. The Magnitude of Burrs Caused by Electrical-Discharge Machining. Master of Science Thesis, Utah State University, Logan, Utah. 1969.

23. Martellotti, M. E. An Analysis of the Milling Process. Transactions of the ASME. 63(8):677-700. November 1941.

24. Merchant, M. E. Metal Cutting Research, p. 5-44. In Machining--Theory and Practice. American Society of Metals, Metals Park, Ohio. 1950.

25. Mulkey, J. R. Strain Hardening Exponent for 17-4 Ph Stainless Steel. Bendix Corporation (Kansas City Division) Report BDX 613-550. October 1971.

26. Nadai, A. Theory of Flow and Fracture of Solios (Vol 1). McGraw-Hill Book Company, Inc., New York. 1950.

27. O'Neill, Hugh. The Hardness of Metals and its measurement. Sherwood Press, Cleveland, Ohio. 1934.

28. Oxford, C. J. Jr. On the Drilling of Metals: 1 Basic Mechanics of the Process. Transactions of the ASME. 77(2):103-114. February 1955.

29. Pond, J. B. Drill Points Assume New Shape. Reprint from Cutting Tool Engineering, circa. 1969.

30. Prager, William, and Philip G. Hodge, Jr. Theory of Perfectly Plastic Solids. Dover Publications Inc. New York. 1968.

31. Seidel, Jurg. R. Machinability Evaluation of Free-Cutting Materials with Specific Reference to Copper Alloys. Proceedings of the International Conference on Manufacturing Technology. Published by American Society of Tool and Manufacturing Engineers. Dearborn, Michigan. pp. 729-746. 1967.

32. Shaw, M. C., and G. J. DeSalvo. A New Approach to Plasticity and its Application to Blunt Two Dimensional Identers. Journal of Engineering for Industry. pp. 649-479. 1970.

33. Strasser, Federico. How Control of Burrs Aids Sheet Metal Stamping. The Iron Age. 185(3):90-92. January 21, 1960.

34. Symonds, P. S. Plastic Shear Deformations in Dynamic Load Problems. In Engineering Plasticity (J Heyman and F. A. Lecke, editors). Cambridge University Press, London. p. 647-664. 1968.

35. Tabor, D. The Hardness of Metals. Oxford University Press, London. 1951.

36. Universal-Cyclops Specialty Steel Division, Stainless Steel, Cyclops Corporation, Bridgeville, Pennsylvania. 1965.

37. Vilenski, D., and M. C. Shaw. The Importance of Wonkpiece Softening on Machinability. Annals of the C. I. R. P. 18:623-631. 1970.

38. Wang, K. K., Khalil Taraman, and S. M. Wu. An Analysis of Punching Variables by Two-Level Fractional Factorial Design. ASME Paper 69-WA/Prod-27. 1969.

39. Wukusik, C. S., and R. S. Zeno. Improving Punchability of Silicon Steel. Tool Engineer, 41(12):63-70. December 1958.

40. Zaima, S., A. Yuki, and S. Kamo. Drilling of Aluminum Alloy Plates with Special Type Point Drill. Journal of Japan Institute of Light Metals. 18(5):269-276. May 1968:18(6):307-313. June 1968.

41. Zorev, N. N. Metal Cutting Mechanics. Pergamon Press, New York. 1966.

APPENDIXES

Appendix A

Derivation of Burr Formulas

Derivation of Roll-Over Burr Equations

The properties of the Roll-Over Burr can be readily calculated using the concept of the Plastic Hinge. Using the principle of least work we postulate that for this plastic process, the material ahead of the cutter will respond to the deformation path requiring the least work. For the conditions shown in Figure A1 the deformation modes of the chip in the vicinity of the shear zone are bending and shearing. To find the point at which bending will occur we equate the work required to bend a beam to the work required to shear the material.

The work required to continue the cutting action through the distance 2h is,

$$W_c = F_c(2h - \delta) + \frac{F_c\delta}{2} \qquad [A1]$$

W_c is the work done in cutting

F_c is the principal cutting force

The first term in [A1] is the work required up to the point where the shear zone intersects the vertical surface of the workpiece (point a in Figure A2). The second term in [A1] is the result of a decreasing shear zone length as the tool moves from g to a'. From the geometry in Figure A2,

$$\delta = \frac{t}{\tan \phi_s} \qquad [A2]$$

where

t = depth of cut

ϕ_s = shear angle

thus

$$W_c = F_c \left[2h - \frac{t}{2 \tan \phi_2} \right] \qquad [A3]$$

The work required to bend the chip as shown in Figure A1 is

$$W_B = \int M_B \, d\Theta \qquad [A4]$$

M_B is the bending moment

Θ is the angle through which M_B acts

$(\Theta = \pi/2 + \gamma)$

γ is the tool rake angle

Following the beam theory developed in elementary strength of materials assume that in a beam of uniform cross section when bent by a moment M_B, cross sections remain plane. Because of bending the longitudinal elements M'P' (Figure A3) lengthen while those on the other side of the neutral axis 00' contract. The strain at any point then is given by

$$\epsilon = Y/\rho \qquad [A5]$$

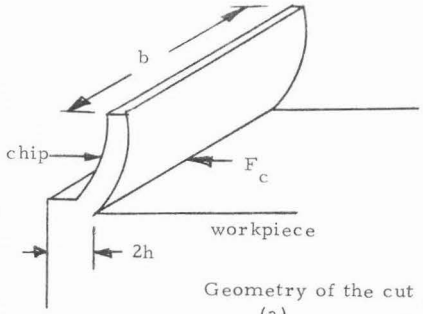

Geometry of the cut
(a)

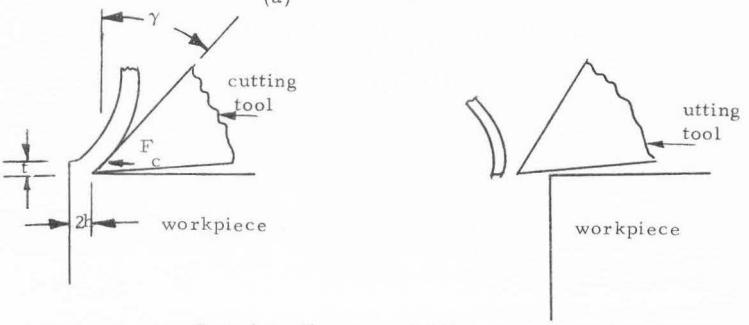

Complete Shearing of Chip
(b)

Plastic Bending of Chip
(c)

Figure A1. Chip Deformation Modes.

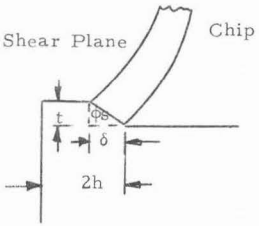

Shear Plane in Cutting
(a)

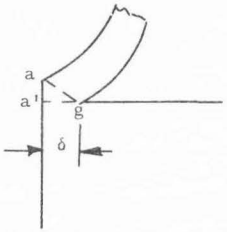

Shear Plane Intersecting Edge
(b)

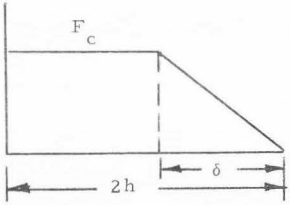

Cutting Distance

Cutting Force as Tool Nears Edge
(c)

Figure A2. Cutting action near edge.

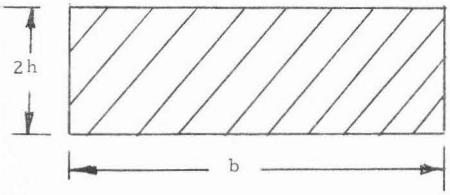

Cross section of beam
(a)

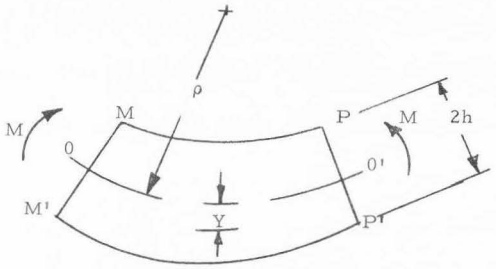

Curvature Produced by Bending
(b)

Figure A3. Beam in bending.

Where Y is the distance from the neutral axis and ρ is the radius of curvature produced by the moment M_B. It is significant to note here that [A5] is valid for plastic deformation as well as for elastic bending.

For a perfectly plastic material such as shown in Figure A4 bending beyond the elastic limit produces plastic stresses in the outer fibers. When the beam is bent such that a fully plastic stress distribution is produced (Figure A4c) it will continue to bend with no additional applied force. Thus Figure A4c represents a plastic hinge condition. The moment which produces this hinge is expressed by

$$M_B = bh^2 \sigma_e \qquad [A6]$$

where σ_e represents the stress at the elastic limit, i.e. the plastic stress.

Since for a perfectly plastic material M_B is independent of Θ

$$W_B = bh^2 \sigma_e \Theta \qquad [A7]$$

To determine the value of h at which bending can occur the two expressions for work are equated. Thus,

$$F_c \left[2h - \frac{t}{2 \tan \phi_s} \right] = bh^2 \sigma_e \Theta \qquad [A8]$$

Applying the quadratic formula to [A8] yields,

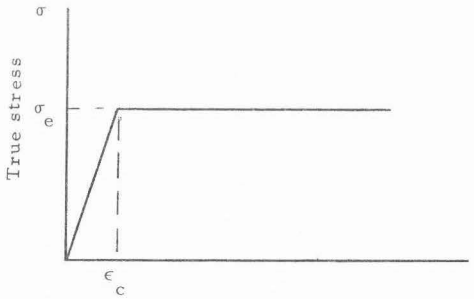

(a)

Perfectly plastic material

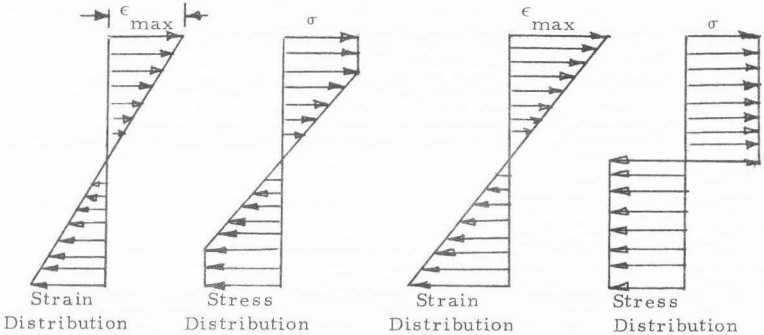

Figure A4. Perfectly plastic behavior.

$$2h = \left[2F_c + \sqrt{4F_c^2 - \frac{2b\sigma_e \Theta t}{\tan \phi_s}} \right] \frac{1}{b\sigma_e \Theta} \qquad [A9]$$

Thus, given the cutting force Fc, the plastic stress of the workpiece, the rake angle of the tool, and the shear angle ϕ, one can estimate the thickness (2h) of the Roll-Over Burr. The value of burr thickness obtained from [A9] will always be an upper limit to burr size because the expression for work in bending neglects the redundant work which occurs in any severe plastic process. Form and Beglinger (10) indicate that 80% of the work performed in cutting is redundant work. If a similar efficiency occurs in bending [A9] will over predict burr size by a factor of 5.

The length of the Roll-Over Burr is approximately equal to the length of cut provided a discontinuous chip is not produced. Because a perfectly plastic material does not strain harden, the hardness of the burr will be the same as for the parent material.

While the analysis for perfectly plastic materials illustrates the concept of the Roll-Over Burr and the plastic hinge, most materials are actually strain hardening. The majority of these materials can be represented by the equation,

$$\sigma = \sigma_o \epsilon^n \qquad [A10]$$

Where σ_o is the stress at a true strain of 1.0 and n is the

strain hardening exponent.

As noted earlier

$$\epsilon = Y/\rho = Yk \qquad [A11]$$

where

$$k = 1/\rho \qquad [A12]$$

The force on half the cross section of a uniform beam in bending is

$$F_b = \int \sigma b dy \qquad [A13]$$

The total moment about the neutral axis is

$$M_B = 2\int_o^h \sigma b y dy \qquad [A14]$$

$$= 2\int_o^h \sigma_o b k^n y^{n+1} dy \qquad [A15]$$

$$= \frac{2\sigma_o b h^{n+2} k^n}{n+2} \qquad [A16]$$

Since at $y = h$ $\epsilon = \epsilon_{max}$ by [A11]

$$\epsilon_{max} = hk \qquad [A17]$$

then

$$M_B = \frac{2\sigma_o bh^2}{n+2} (\epsilon_{max})^n \qquad [A18]$$

A prior however, we do not know either ϵ_{max} or k. From our earlier expression for perfectly plastic materials we could assume

$$\frac{\sigma_o(\epsilon_{max})^n}{n+2} \geq \sigma_y \qquad [A19]$$

Where σ_y is the yield stress (plastic stress for a perfectly plastic material). As an upper limit we note that $\epsilon_{max} \leq \epsilon_{fracture}$. Thus

$$2\sigma_y bh^2 \leq M_B \leq \frac{2\sigma_o bh^2(\epsilon_f)^n}{n+2} \qquad [A20]$$

where ϵ_f = true strain at fracture

Dividing through by $2bh^2$

$$\sigma_y \leq \frac{M_B}{2bh^2} \leq \frac{\sigma_o(\epsilon_f)^n}{n+2} \qquad [A21]$$

Table A1, lists some representative strain hardening values.

Table A1. Strain hardening data[a]

Material	Condition	σ_o (PSI)	n	ϵ_f	σ_y	$\frac{\sigma_o(\epsilon_f)^n}{n+}$
303 S.S.	Annealed	205,000	.51	1.16	35,000	82,000
202 S.S.	1900°1 hr	195,000	.3	1.00	55,000	85,000
17-4phSS	1100°	260,000	.01	.65	160,000	130,000
17-4phSS	900°	320,000	.218	.5	160,000	100,000
1018		90,000	.25	1.05	40,000	40,000

[a] The data in this table was compiled from several sources. These sources include Datsko(7), Kalpakjian(19), Mulkey(25), and Merchant(24).

To find ϵ_{max} in terms of known quantities the work done in bending is found by integrating [A18]. Then an expression is derived for the average bending moment and the work done by this moment is equated to the previous work expression. ϵ_{max} is thereby expressible as a function of Θ.

The work expended in bending is

$$W = (\text{volume of plastic hinge}) \int \sigma d\epsilon \qquad [A22]$$

$$= (\text{vol})\, \sigma_o \epsilon^n d\epsilon \qquad [A23]$$

From [A11] and [A17]

$$\epsilon = \left(\frac{\epsilon_{max}}{h}\right) Y \qquad [A24]$$

$$d\epsilon = \left(\frac{\epsilon_{max}}{h}\right) dY \qquad [A25]$$

thus

$$W = (\text{vol}) \int_o^h \sigma_o \left(\frac{\epsilon_{max}\, Y}{h}\right)^n \frac{\epsilon_{max}}{h}\, dy = \frac{(\text{Vol})\sigma_o \epsilon_{max}^{1+n}}{h^{n+1}} \int Y^n dy \quad [A26]$$

$$= \left(\frac{\text{vol}\,\sigma_o}{n+1}\right) \left(\frac{\epsilon_{max}}{h}\right)^{1+n} h^{n+1} \qquad [A27]$$

Assuming a volume of 2h x 2h x b

$$W = \frac{4b\, h^2 \sigma_o (\epsilon_{max})^{n+1}}{n+1} \qquad [A28]$$

an average moment $\bar{M}_B$ can be expressed as

$$\bar{M}_B = \frac{\int M_B \, d\epsilon'_{max}}{\int d\epsilon'_{max}} \qquad [A29]$$

$$= \frac{\int \left(\frac{2\sigma_o bh^2}{n+2}\right)\left(\epsilon'_{max}\right)^n d\epsilon'_{max}}{\int d\epsilon'_{max}} \qquad [A30]$$

$$\bar{M}_B = \frac{2\sigma_o bh^2 \left(\epsilon'_{max}\right)^n}{(n+2)(n+1)} \qquad [A31]$$

Assuming that the actual strain is somewhere close to the strain at fracture (ϵ_f), $\bar{M}_B$ becomes,

$$\bar{M}_B = \frac{2\sigma_o bh^2 \epsilon^n_f}{(n+2)(n+1)} \qquad [A32]$$

Since n is positive we note that the average moment falls within the bounds required by [A21]. Furthermore experience indicates that the assumption concerning strain at fracture is realistic (many burrs break off when touched).

From [A28] and [A4]

$$\frac{4 bh^2 \sigma_o (\epsilon_{max})^{n+1}}{n+1} = \int \bar{M}_B \Theta = \bar{M}_B \Theta$$

$$= \frac{2\sigma_o bh^2 \epsilon^n_f \Theta}{(n+2)(n+1)} \qquad [A33]$$

$$\epsilon_{max} = \left[\frac{\epsilon_f^n \Theta}{n+2} \right]^{1/n+1} \qquad [A34]$$

thus

$$W = \frac{4bh^2 \sigma_o \epsilon_f^n}{(n+1)} \left[\frac{\Theta}{n+2} \right] \qquad [A35]$$

using [A3] and the quadratic formula

$$2h = \left[2F_c + \sqrt{4F_c^2 - \frac{8b \sigma_o \epsilon_f^n t \Theta}{(n+1)\tan\phi_s(n+2)}} \right] \left[\frac{(n+1)(n+2)}{4b \sigma_o \Theta \epsilon_f^n} \right] \qquad [A36]$$

Equation [A36] is the expression for Roll-Over Burr thickness in a strain hardening material.

The cutting force F_c in orthoginal turning can be expressed by[1]

$$F_c = tb \sigma_s \left[\text{Tan} \frac{(C+\tau-\gamma)}{2} + \text{cotan} \frac{(c-\tau+\gamma)}{2} \right] \qquad [A37]$$

Where

σ_s = shear strength of the workpiece

γ = rake angle of tool

τ = friction angle = $\tan^{-1}\lambda$

t = depth of cut

b = width of cut

C = material machining constant

λ = coefficient of friction

ϕ_s = shear angle = $\frac{C-\tau+\gamma}{2}$

[1] Several authors including Kronenberg(20) and Zorev(41) present more accurate expressions for F_c, but the expression given is considerably easier to visualize and is within 20% of the more precise formulas.

To illustrate the impact of the machining parameters of the size of the burr [A9] will be used. At most

$$2h = \frac{4 F_c}{b \sigma_e \Theta} = \frac{4 t \sigma_s}{\sigma_e \Theta} \text{ (function of angles)} \qquad [A38]$$

Thus an increasing depth of cut t should increase the burr thickness. Decreasing the rake angle should increase the burr thickness since $\Theta = 90^{\circ}$ + rake angle. Materials with high shear strengths should also have thicker burrs than materials with low shear strengths. Since F_c increases as a tool dulls, burrs should get thicker as the tool wears. Each of these effects have in fact been qualitatively observed in production.

Two additional aspects of [A37] and [A38] are noteworthy. For one dimensional stresses in a perfectly plastic material von Mises yield condition predicts $\sigma_s = \sqrt{1/3}\, \sigma_e$. Thus from [A38] the ratio σ_s / σ_e is a constant. For strain hardening materials however, the ratio is a function of the strain in the material. The function of angles indicated in [A37] and [A38] are a function of the cutting conditions. The magnitude of this function can vary greatly between different machining conditions. The function is therefore a very significant part of the equation. The values for C and τ can be obtained from sources such as Kronenberg (20) and Merchant (24) or can be easily determined from measurements of chip thickness.

The hardness of a strain hardening material is a function of the strain in the material. From [A34] one observes that the strain in the outer fibers (ϵ_{max}) is,

$$\epsilon_{max} = \epsilon_f^{n/n+1} \left(\frac{\Theta}{n+2}\right)^{1/n+1} \qquad [A39]$$

Table A2 lists some representative values of ϵ_{max}. As indicated there the strain in the outer fibers approaches the strain

Table A2. Strain in bending.

Material	n	E_f	Θ	ϵ_{max}
303 Se st. st. (annealed)	.51	1.16	90^o	1.15
"	.51	1.16	115^o	1.34
17-4ph st. st. (H-900)	.218	.5	115^o	0.81
1018	.25	1.05	115^o	1.02
202 S.S. (1900^o 1 hr)	.3	1.00	115^o	0.9

required to fracture a tensile specimen. In the case of 17-4ph st. st. The burr would fracture before it was bent out of the path of the cutter. Similar results would be noticed for any non-strain hardening material.

As noted by Kalpakjian (19) the Meyer Hardness Number (MHN) can be expressed by

$$MHN = 2.8\sigma_y \qquad [40]$$

where σ_y is the yield strength of the material. From [A10] this reduces to

$$MHN = 2.8\ \sigma_o\ \epsilon^n \qquad [A41]$$

In the annealed condition the Brinell Hardness Number of 303Se stainless steel is BHN 160[1]. At maximum strain it is BHN 475. An average hardness across the burr would therefore be

$$\bar{H} = 1/2\ (H_{initial} - H_{final}) \qquad [A42]$$

$$\bar{H} = 1/2\ (160 + 475) = \text{BHN } 317$$

And for cold drawn material the initial material hardness would be BHN 228 which gives an average burr hardness of BHN 351. Previous studies by the author (12) found that measured hardnesses of the burrs were BHN 388 for a parent material hardness of BHN 227. Thus [A42] does predict the burr hardness very accurately.

As indicated earlier the length of the Roll-Over Burr is a function of the machining process. In end milling it will be equal to the radial depth of cut provided the radial depth to diameter ratio is less than 2/3. For ratios larger than this the burr length will be approximately 2/3 of the cutter diameter. In side milling the burr length will be equal to radial depth of cut.

---

[1] See for example reference (36). Brinell Hardness Values are used here rather than Meyer Hardness Numbers since most of the published material properties use the more familiar BHN. Equations [A41] illustrates the basic concept that hardness is directly related to strain. Equation [A42] utilizes published values which are readily available.

Derivation of the Poisson Burr Equations

As indicated earlier in this study the Poisson Burr is formed at right angles to the applied force. In simple compression, bulging occurs at the sides of specimen as a result of Poisson's ratio. In plastic deformation, to maintain constant volume, material continues to push further out the sides of the specimen and will not retract when the applied force is released. In metal cutting the applied force is distributed by a quasi-knife edge and the bulge is continuously formed and sheared as the tool advances into the workpiece. (Figure A5) This severed bulge is the burr common to most milling and turning operations.

Consider the force and stress distribution at the cutting edge of a tool. Although raxor sharp to the naked eye, a small radius actually exists on this edge. In addition as pointed out by Form (10) and others a small buildup of material occurs at this edge producing a larger effective cutting edge radius. (Figure A6) At the cutting edge (or at the effective radius) then a nearly radial stress distribution exists.

Assuming the stress distribution is radial when we instantaneously freeze the cutting process a cylinder of material centered at the cutting edge radius is sufficient to define the stress system. Actually as shown in Figure A7 only a semi-cylinder exists around the cutting tool. The

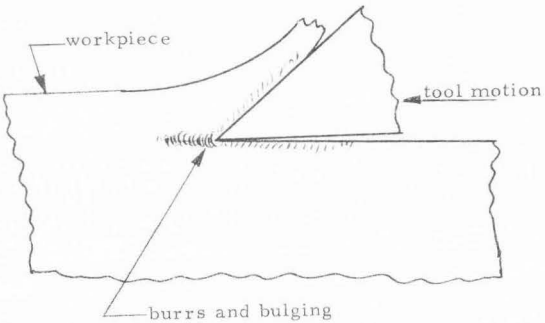

Figure A5. Burrs and bulging in chip formation.

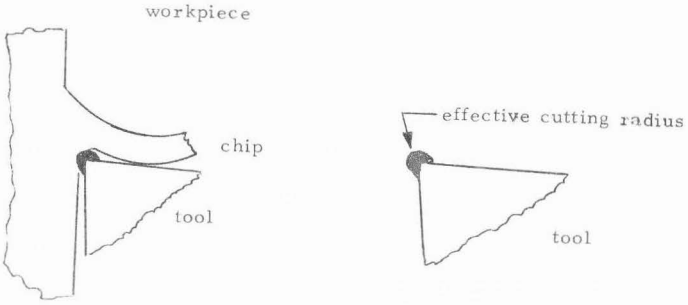

Figure A6. Cutting tool action.

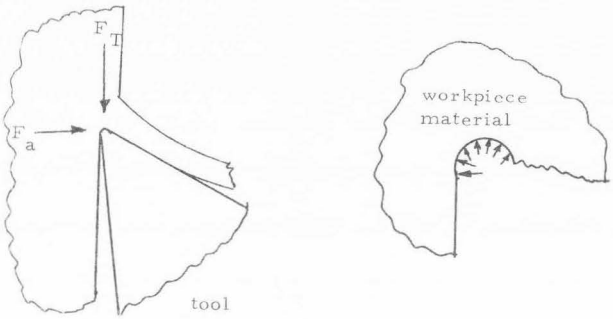

Figure A7. Assumed stress distribution at effective cutting radius.

chip and the workpiece, however, provide a tensile restraint similar to that produced by one-half of a pressurized cylinder on the other half. Effectively then our stress model is that of a pressurized cylinder as shown in Figure A8.

Consideration of the force equilibrium required on a small element of the cylinder (Figure A9) results in the following equations.[1]

$$\frac{\partial \sigma_r}{\partial r} + \frac{1}{r}\frac{\partial \sigma_{r\theta}}{\partial \theta} + \frac{\partial \sigma_{rZ}}{\partial z} + \frac{\sigma_r - \sigma_\theta}{r} = 0 \qquad [A43]$$

$$\frac{\partial \sigma_{rz}}{\partial r} + \frac{1}{r}\frac{\partial \sigma_{\theta z}}{\partial \theta} + \frac{\partial \sigma_z}{\partial z} + \frac{\sigma_{rz}}{r} = 0 \qquad [A44]$$

$$\frac{\partial \sigma_{r\theta}}{\partial r} + \frac{1}{r}\frac{\partial \sigma_\theta}{\partial \theta} + \frac{\partial \sigma_{\theta z}}{\partial z} + \frac{2\sigma_{r\theta}}{r} = 0 \qquad [A45]$$

by definition

$$\epsilon_r = \frac{\partial u}{\partial r}, \qquad \epsilon_\theta = \frac{u}{r} + \frac{\partial v}{r\,\partial \theta}, \quad \epsilon_z = \frac{\partial w}{\partial z} \qquad [A46]$$

$$\epsilon_{r\theta} = \frac{\partial u}{r\,\partial \theta} + \frac{\partial v}{\partial r} - \frac{v}{r}, \quad \epsilon_{rz} = \frac{\partial u}{\partial z} + \frac{\partial w}{\partial r} \qquad [A47]$$

$$\epsilon_{z\theta} = \frac{\partial v}{\partial z} + \frac{\partial w}{r\,\partial \theta} \qquad [A48]$$

The terms u, v, and w in the above equations indicate displacements in the radial, tangential, and longitudinal directions. We shall

[1] Body forces are assumed to be zero.

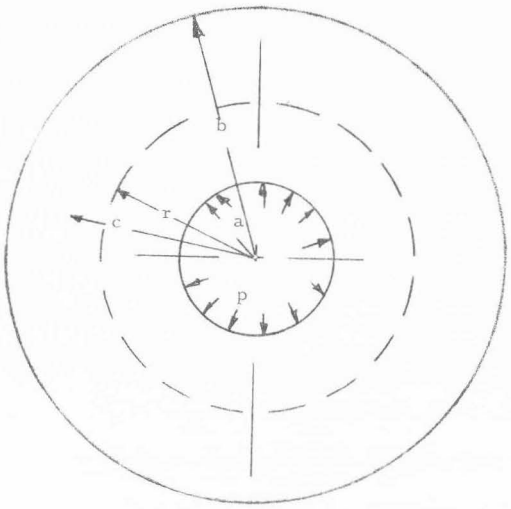

Figure A8. Geometry of equivalent pressurized cylinder.

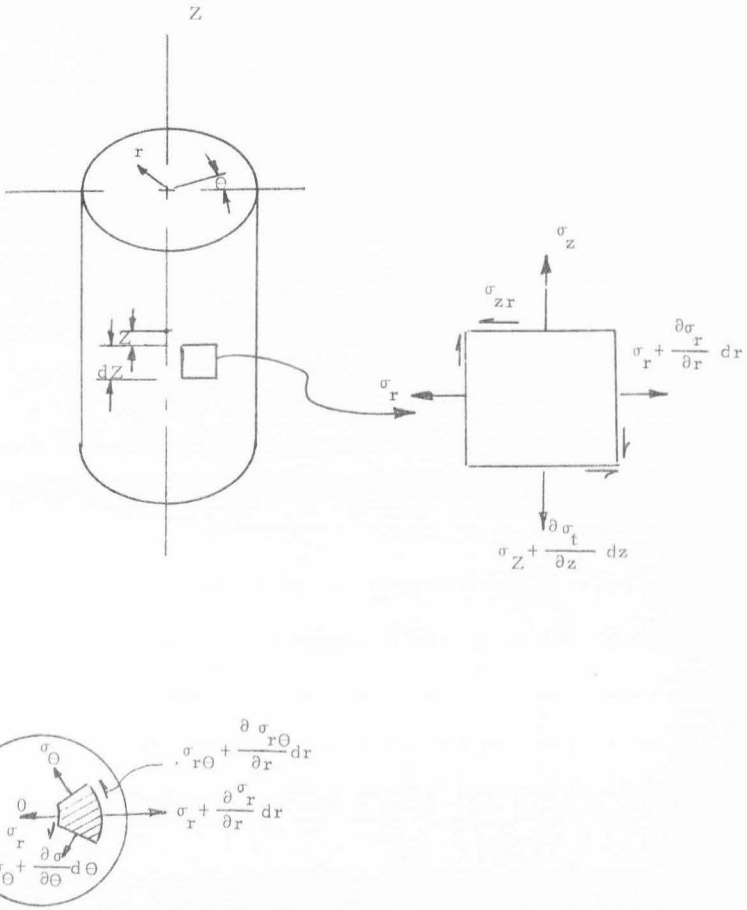

Figure 9. State of stress on an infinitesimal element.

assume small strains occur, recognizing that if large strains occur coordinates of the strained system should be employed, rather than unstrained coordinates.

We note that the geometry involved requires that σ_z and σ_r must be independent of Θ. Since we are concerned in finding plastic deformations and not stresses we will assume that a condition of plane stress exists such that $\sigma_z = 0$. Similarly all shear forces are assumed negligible and the remaining principle stresses are assumed independent of z. The resulting equations become

$$\sigma_r - \sigma_\Theta + r \frac{\partial \sigma_r}{\partial r} = 0 \qquad [A49]$$

$$\epsilon_r = \frac{\partial u}{\partial r} \qquad [A50]$$

$$\epsilon_\Theta = \frac{u}{r} \qquad [A51]$$

$$\epsilon_z = \text{const} \qquad [A52]$$

In the addition to the previous equations in plastic deformation the total volume of material must remain constant. Thus

$$\epsilon_r + \epsilon_\Theta + \epsilon_z = 0. \qquad [A53]$$

Using von Mises Distortion Energy Criteria to define the conditions for material flow gives

$$\left[\frac{1}{2}(\sigma_r - \sigma_\Theta)^2\right]^{1/2} = \sigma_a = \sigma_{yield} \qquad [A54]$$

$$\text{or}\quad \sigma_r^2 - \sigma_\Theta \sigma_r + \sigma_\Theta^2 = \sigma_a^2 = \sigma^2_{yield} \qquad [A55]$$

Where σ_{yield} is the yield strength of a perfectly plastic material.[1]

The following solution is taken directly from Nadai's work (55). For further details of the solution the reader is referred to that reference.

Equation [A55] is the equation of an ellipse of whose path defines radial and tangential stress combinations which provide plastic flow. (Figure A10) The major and minor semi axis are $\sqrt{2}\,\sigma_a$ and $\sqrt{2/3}\,\sigma_a$. By defining two new stresses σ and σ' such that

$$\sigma = \frac{\sigma_\Theta + \sigma_r}{\sqrt{2}} = \sqrt{2}\,\sigma_0 \sin\phi,$$

$$\sigma' = \frac{\sigma_\Theta - \sigma_r}{\sqrt{2}} = \sqrt{\frac{2}{3}}\,\sigma_o \cos\phi, \qquad [A56]$$

Where ϕ is defined as shown in Figure A10, we obtain new expressions for σ_r and σ_Θ:

$$\sigma_r = \frac{\sigma - \sigma'}{\sqrt{2}} = \frac{2\sigma_a}{\sqrt{3}} \sin(\phi - \tfrac{\pi}{6}),$$

$$\sigma_\Theta = \frac{\sigma + \sigma'}{\sqrt{2}} = \frac{2\sigma_a}{\sqrt{3}} \sin(\phi + \tfrac{\pi}{6}). \qquad [A57]$$

---

[1] The approach at this point is to assume that the strain hardening of a material can be effectively defined by some effective perfectly plastic yield strength. Ford (9) presents a numerical technique which could be used to obtain more accurate results for strain hardening materials. The use of this method however is beyond the scope of this study. In addition the numerical methods tend to obscure the actual phenomena which occurs. Brigeman(4) and Nadai (26) also discuss strain hardening effects.

By substituting [A57] into [A49] the following is obtained

$$r \frac{\partial}{\partial r} \sin(\phi - \pi/6) = \cos\phi \qquad [A58]$$

Integrating [A58] gives

$$\frac{C_1^2}{r^2} = e^{-\sqrt{3}\phi} \cos\phi \qquad [A59]$$

Where C_1 is a constant of integration.

Referring to Figure A11, we note that a plastic zone exists between the points $a \leq r \leq c$ while for $r \geq c$ an elastic state exists. The stresses in the elastic region are given by

$$\sigma_\Theta = -\sigma_r = \frac{\sigma_a c^2}{\sqrt{3}\, r^2} \qquad [A60]$$

The elastic radial displacement is given by

$$u = \epsilon_r r = \frac{(1+\nu)\,\sigma_a\, c^2}{\sqrt{3}\, Er} \qquad [A61]$$

Since the elastic plastic interface must be compatible, by [A60] for r=c [A59] becomes

$$\frac{C_1^2}{c^2} = e^{-\sqrt{3}\phi} \cos\phi \qquad [A62]$$

From Figure A10 however, $\phi_c = 0$ where subscript c implies the value of r=c. Thus from [A62] $c_1 = c$. At r=a, [A62] becomes

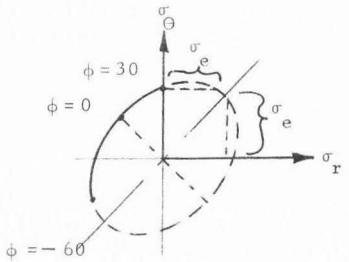

Figure A10. Ellipse of plasticity.

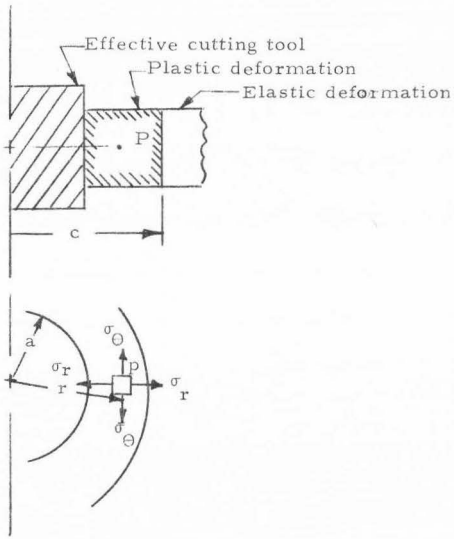

Figure A11. Deformation of workpiece.

$$c^2 = a^2 e^{-\sqrt{3}\phi_a \cos \phi_a} \qquad [A63]$$

Thus ϕ_a is determined by the ratio c/a. Since at r=a $\sigma_r = -p$ and $\phi = \phi_a$, by [A57]

$$P = \frac{2\sigma_a}{\sqrt{3}} \sin(\pi/6 - \phi_a) \qquad [A64]$$

Assuming now that in the plastic region the following relationships apply.

$$\epsilon_r = \frac{du}{dr} = \psi(\sigma_r - \frac{\sigma_\Theta}{2}) \qquad [A65]$$

$$\epsilon_\Theta = \frac{u}{r} = \psi(\sigma_\Theta - \frac{\sigma_r}{2}) \qquad [A66]$$

note that ψ is an unknown flow function.

The quantity $\epsilon_r - \epsilon_\Theta$ can be expressed as

$$\epsilon_r - \epsilon_\Theta = r \frac{d\epsilon_\Theta}{dr} \qquad [A67]$$

substituting [A65] and [A66] into [A67] gives

$$r \frac{d}{dr} \psi(2\sigma_\Theta - \Theta_r) = 3\psi(\sigma_r - \sigma_\Theta) \qquad [A68]$$

using [A57], [A68] becomes

$$r \frac{d}{dr} \psi\left[2\sin(\phi + \pi/6) - \sin(\phi - \pi/6)\right] = 3\psi\left[(\sin(\phi - \pi/6) - \sin(\phi + \pi/6)\right] \qquad [A69]$$

making the required trigametic substitutions and using the fact that

$$\frac{\partial}{dr} = \frac{\partial}{\partial \phi} \frac{d\phi}{dr} \qquad [A70]$$

in conjunction with [A59], [A69] reduces to

$$\frac{d\eta}{d\psi} = -\sqrt{3}\,\psi \qquad [A71]$$

where

$$\eta = \psi\left[\cos(\phi - \pi/6)\right] \qquad [A72]$$

thus

$$\eta = Coe^{-\sqrt{3}\phi} \qquad [A73]$$

and

$$\psi = \frac{Coe^{-\sqrt{3}\phi}}{\cos[\phi - \pi/6]} \qquad [A74]$$

then

$$\epsilon_r = -C_o\sigma_o \frac{e^{-\sqrt{3}\phi}\cos[\phi + (\pi/6)]}{\cos[\phi - (\pi/6)]}\,,$$

$$\epsilon_\Theta = C_o\sigma_o e^{-\sqrt{3}\phi}. \qquad [A75]$$

Since [A75] must also be valid at the plastic-elastic interface equating [A75] to [A61] and noting that at r=c, $\sigma_r = -\sigma_\Theta$, C_o is found as

$$C_o = \frac{1+\nu}{\sqrt{3}\,E} \qquad [A76]$$

From [A59] and [A63]

$$\frac{r^2}{a^2} = \frac{e^{-\sqrt{3}(\phi a - \phi)} \cos \phi_A}{\cos \phi} \qquad [A77]$$

since

$$u = \epsilon_\Theta r = C_o \sigma_a r e^{-\sqrt{3}\phi} \qquad [A78]$$

then at r=a

$$u_a = C_o \sigma_a a e^{-\sqrt{3}\phi_a} \qquad [A79]$$

$$= \frac{(1+\nu)}{\sqrt{3}E} \sigma_a a e^{-\sqrt{3}\phi_2} \qquad [A80]$$

as noted before P at this point is

$$P = \frac{2\sigma_a}{\sqrt{3}} \sin(\pi/6 - \phi_a) \qquad [A81]$$

since

$$\epsilon_r + \epsilon_\Theta + \epsilon_z = 0$$

$$\epsilon_z = -\epsilon_r - \epsilon_\Theta$$

$$= \frac{C_o \sigma_a e^{-\sqrt{3}\phi} [\cos(\phi+\pi/6)]}{\cos[\phi - \pi/6]} - C_o \sigma_a e^{-\sqrt{3}\phi}$$

$$= C_o \sigma_a e e^{-\sqrt{3}\phi} \frac{[\cos(\phi+\pi/6) - \cos(\phi - \pi/6)]}{\cos(\phi - \pi/6)} \qquad [A82]$$

From [A79]

$$\epsilon_z = \frac{u_a}{a}\left[\frac{\cos(\phi + \pi/6) - \cos(\phi - \pi/6)}{\cos(\phi - \pi/6)}\right]$$

noting $\sin\phi \sin \pi/6 = .5(\cos[\phi - \pi/6] - \cos[\phi + \pi/6])$

and $\cos(\phi - \pi/6) = \cos\phi \cos \pi/6 + \sin\phi \sin \pi/6$

$$\epsilon_z = \frac{u_a}{2a}\left(\frac{-\sin\phi \sin \pi/6}{\cos\phi \cos \pi/6 + \sin\phi \sin \pi/6}\right)$$

$$= \frac{u_a}{2a}\left[\frac{.5 \sin\phi}{\frac{\sqrt{3}}{2}\cos\phi + \frac{1}{2}\sin\phi}\right]$$

$$= \frac{u_a}{a}\left[-\frac{1}{2}\frac{\sin\phi}{\left(\sqrt{3}\cos\phi + \sin\phi\right)}\right] \qquad [A83]$$

Define $\Delta h = h\epsilon_z$ [A84]

Δh is plotted as Δ function of angle ϕ and P/σ_o in Figure A12. The quantity Δh is the burr height (or length). The dimension c represents the burr width.

From [A65]

$$c = \left[a^2 e^{-\sqrt{3}\phi_a \cos\phi_a}\right]^{1/2}$$

$$\phi_a = -\sin^{-1}\left(\frac{\sqrt{3}P}{2\sigma_a}\right) + \frac{\pi}{6} \qquad [A85]$$

$$\Delta h = \frac{h(1+\nu)\sigma_a e^{-\sqrt{3}\phi_a}}{\sqrt{3}E}\left[-\frac{1}{2}\cdot\frac{\sin\phi}{\left(\sqrt{3}\cos\phi + \sin\phi\right)}\right]$$

$$w = c - a = a\left[e^{-\sqrt{3}\phi_a \cos\phi_a} - 1\right]$$

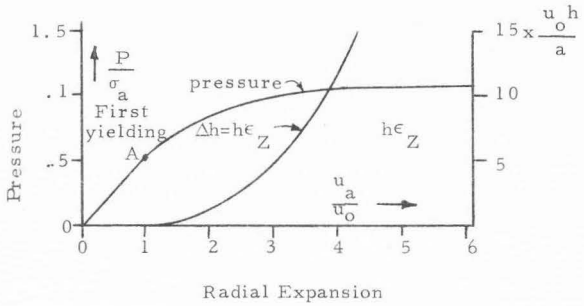

Figure A12. Plastic expansion of a hole.

Two significant factors result from this analysis:

1. The problem is entirely specified for any material given the cutting edge radius a and the cutting edge pressure P.
2. Feedrates and cutting speeds do not appear in any of the equations.

For normal machining conditions it is not unreasonable to assume that strain rate effects are constant. Thus the effect of speed would be small. The analysis presented can only apply when the depth of cut (or feedrate in the case of turning) is sufficiently large such that radial flow presents more resistance than axial flow. On very shallow cuts it is easy to visualize that resistance on the cutting shear plane is lower than that required to push material along the axis of the cutting edge radius. Under the specified conditions then neither feedrate nor spindle speed should influence burr properties. Essentially this implies that for a given material the ratio P/σ_a is a constant. Thus the burr properties are a function of the cutting edge radius and the workpiece material properties.

Zorev's work (41) adds an interesting sidelight to the value of cutting pressure P at the cutting edge. Using cutting edge radii varying from 'zero' to 0.040 inch he noted a decrease in cutting forces with larger radii. A logical but erroneous assumption that could easily occur here is that burr size should also decrease if the forces decreases As indicated in the present analysis burr thickness w should increase in proportion to the cutting radius. As indicated by Zorev although

cutting forces decreased the cutting pressure remained constant or increased slightly.

When the depth of cut is small the only way a Poisson Burr can form is for the flank surface to squeeze material along the axis of the cutting edge. Figure A13 illustrates this effect. Although this 'ironing' action of the flank surface was observed to be the cause of Poisson Burrs at freerates of .002 to .004 ipr an analytical analysis of this deformation mode was not made, since it was not observed until the end of the study. The material flows vertical out of the plane of the paper rather than backwards because the material behind the tool is highly work hardened and offers more resistance to flow than does the material in the vertical direction.

The values of ϕ in equations [A56] through [A85] depend upon the state of stress within the body. In Figure A10, a value of $\phi = 30^{o}$ represents the case of no radial stress. At $\phi = -30^{o}$ only radial stress exists at a point. By the definition of the problem the stress at the inner radius a is not all radial since plastic yielding has occured. As a result $\phi = -60^{o}$. Within the elastic zone the tangential and radial stresses must be equal thus at the interface (r=c) $\phi = 0^{o}$. Thus any point in the plastic zone will be associated with an angle ϕ between 0^{o} and -60^{o}. Nadai (26) presents graphs of the principal stresses which are convenient for finding the actual stress distribution within the plastic zone.

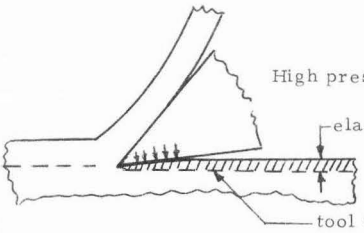

Elastic and thermal expansion
(a)

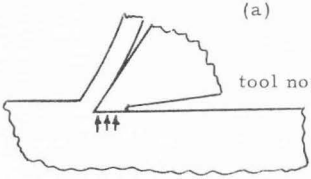

Plastic deformation of tool
(b)

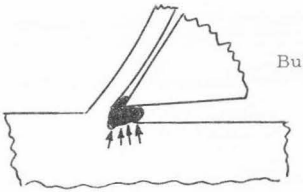

Built up edge rubs workpiece
(c)

Pressure on the flank surface pushes material vertically out of the plane shown.

Figure A13. Sources of flank pressure.

Analysis of the Entrance Burr

The Poisson Burr described on the previous pages occurs after the tool begins cutting. Another related burr occurs at the point at which the tool first contacts the workpiece. To analyze this entrance burr it is convenient to consider first the indentation of a wedge into a workpiece. As shown in Figure A14 a lip of metal is pushed up at the sides of the wedge when it enters the material. By geometry, the volume of the material in the two lips must equal the volume of that portion of the wedge which is in the workpiece. For a perfectly plastic material the height of these lips and the dimension b and angle β are given by:

$$h = \frac{t \sin (\beta - \alpha)}{\cos \beta - \sin (\beta - \alpha)} \qquad [A86]$$

$$\beta = \frac{1}{2}\left\{\alpha + \cos^{-1} \tan (\pi/4 - \frac{\alpha}{2})\right\} \qquad [A87]$$

$$b = t \sin (\beta - \alpha) \frac{\sin \beta + \cos (\beta - \alpha)}{\cos \beta - \sin (\beta - A)} \qquad [A88]$$

As Dugdale (8) and Shaw and De Salvo (32) point out however strain hardening materials will exhibit smaller displacements than indicated by [A86]. The effect of strain hardening on the size of the lip is best illustrated by work performed on spherical indenters. O'Neill's (27) Foss's (11), and Tabor (35) work indicate that the piling up effect shown in Figure A14 only occurs in nonstrain hardening materials. Materials which strain harden exhibit a depression

[1] An extensive treatment of wedge indentation is given by Prager and Hodge (30).

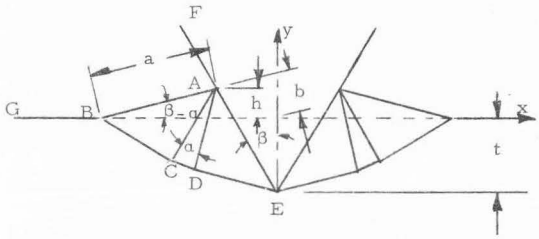

Figure A14. Displacements produced by lubricated wedge in perfectly plastic material.

rather than a raised lip. (Figure A15) The material which is displaced forms a small mound at some distance away from the tool-workpiece interface.

As shown in the following table from O'Neill's text (27) a Meyer exponent of 2.34 appears to be the dividing line between the tendancy to pile-up or to sink-in. Meyer's exponent n' is related to the strain hardening exponent by,

$$n = n' - 2.0 \qquad [A89]$$

Thus a material with a strain hardening exponent of .34 should form little or no burr. Merchant's data (24) indicate that 303S stainless steel has a Meyer Hardness Exponent of 2.37 in the hot rolled condition. One would therefore predict that little burr would form at the edge of

Table A3. Ridge effect and Meyer n' value.

Material	Percentage sinking in (−) or piling-up (+)	n'
MAGNESIUM, cast	−22	2.42
ALUMINIUM, rolled and annealed	− 4	2.32
" cold-hammered 90% reduction	+30	1.96
COPPER, cast	−27	2.58
" rolled and annealed at 900°C.	−23	2.50
" rolled and annealed at 600°C.	− 8	2.34
" cold-hammered 20% reduction	+28	2.01
" cold-hammered 75% reduction	+28	1.96
BRASS, 62-5 Cu, 2-6 Pb	0	--
" cold-worked	+ 6.5	--
STEEL		
Mild steel, annealed	+10	2.22
Manganese steel. d/D = 0-6	+ 2	2.30

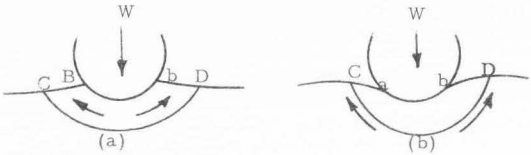

(a) For highly worked metals, (i.e., non strain hardenable) the flow of metal around the indenter produces 'piling-up', (b) for annealed metals the displacement of metal occurs at regions at a small distance from the indenter so that 'sinking-in' occurs.

Figure A15. Material displacement using spherical indenters.

indentation for this material. Similarly since 1014 and 52100 steels in the cold drawn condition have n' values of only 2.16, one would expect a noticeable burr at the indentation edge.

As discussed earlier the cutting edge of a tool can be treated as a long cylinder. The indentation of cylinders into flat workpieces for accurate preductions of burr formation at the entrance of a cut an analytical treatment is needed. Intuitively it appears that the piling-up tendancy of a cylinder would lie somewhere between that of an infinite wedge and that of a sphere. Until such analysis are made one is obliged to use the strain hardening exponent (or Meyer Hardness Exponent) as an indicator.

Derivation of Tear Burr Equations

The Tear Type Burr does not lend itself to ready analysis. As shown in Figures 10(b) and 13(a) it is primarily the result of a tensile or shear failure at a yield hinge in the majority of machining cuts the chip undergoes shear on the shear in front of the tool. This results in a chip which is thicker than the depth of cut. As a result slip on the shear plane is occuring at or near the same time that the tear burr is forming.

For a conceptual model however one can assume that the chip is a solid rectangular beam held between two rigid clamps. (Figure A16) Let the beam depth be h and the beam thickness be b. At time t_o an impulsive load is applied to the beam. The velocity of the impulse load is V_o. Since the chip will be sheared off the impulse force is equated to the force required to shear the beam

$$Q_p = \sigma_s bh \qquad [A90]$$

where

$$Q_p t = mV_o \qquad [A91]$$

Q_p is the plastic shearing force (an impulse force)

M is the effective mass of the cutter tooth

V_o is the tooth velocity

For a perfectly plastic material the plastic bending stress will be

$$M_p = \frac{bh^2}{4} \sigma_p \qquad [A92]$$

At this point suppose shear flow occurs when the shear force reaches Q_p in magnitude and that this occurs independent of the bending moment.[1] After manipulation Symond (34) shows that the quantity $Q_p L/ZMp$ is

$$\frac{Q_p L}{2M_p} = \frac{4bh\,\sigma_s L}{2bh^2\sigma_p} = \frac{z\,\sigma_s L}{\sigma_p h} \qquad [A93]$$

The quantity $\frac{2\sigma_s}{\sigma_p}$ is a constant for any perfectly plastic material. Using the von Mises criteria $\sigma_s = 1/2\,\sigma_p$. Thus

$$\frac{Q_p L}{2M_p} = \frac{L}{h} \qquad [A94]$$

For a 1/4" wide side cut and a .002 thick chip [A94] would be 60. For a close to 1.0 which corresponds to a fully loaded beam the ratio of shearing energy to total initial energy is in the order of .05. (Figure A15) This essentially implies that the majority of work performed in removing this chip, is spent in bending. The energy required to shear this chip is

---

[1] The reader is referred to Symond's paper for an in depth discussion of the reason for this assumption. Essentially the rationale is based on independent hinges which however can be related through expressions for impact time.

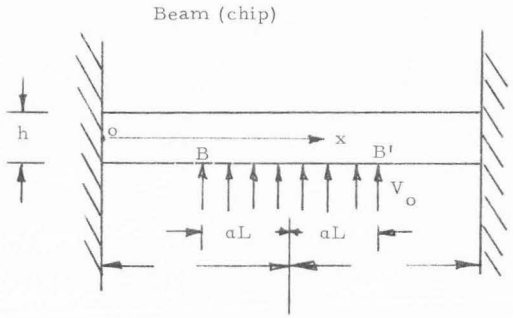

Figure A16. Idealized model of chip.

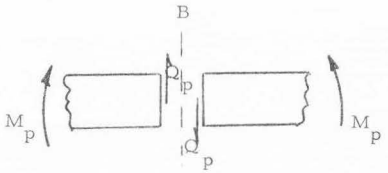

Figure 17. Free body diagram at point B.

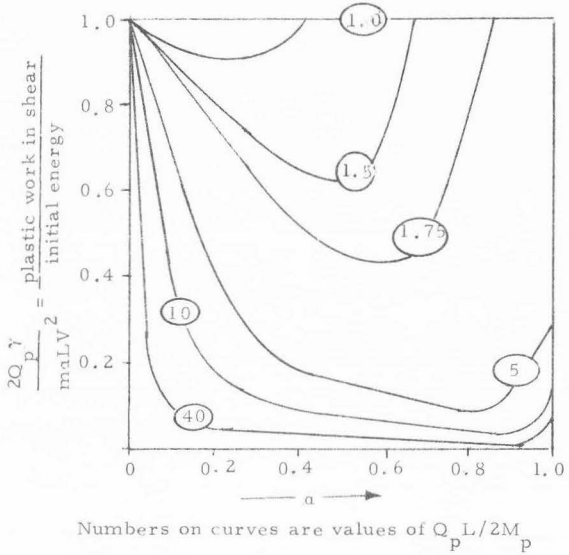

Figure A18. Plastic work in shear.

$$E_s = 2\Omega_p(h) = 2\sigma_s bh^2 \qquad [A95]$$

The plastic bending stress then consumes $\frac{95}{5}(2\sigma_s bh^2)$ or

$$E_b = 38\sigma_s bh^2 \qquad [A96]$$

Essentially then this simplified analysis indicates that the tear burr can be considered similar to the Roll-Over Burr. For shallow depths of cut the burr rolls over onto the top surface. (Figure A19) Heavier depths of cut decrease the L/h ratio which increases the percentage of work expended in shearing. Thus the burr formation modes should change with deeper depths of cut. For shallow cuts this analysis implies that burr thickness should be close to the depth of cut h. The length of burr is not determined by the method used here, but by the nature of the model and physical reality it should be in the order of the depth of cut. Burr hardness should be expressible by [A42].

The assumptions of perfectly plastic material, rectangular chip shape, and lack of influence from the shearing planes which occur in chip formation limit the quantitative utility of this approach. It does emphasize however the significance of bending moments in the burr formation process.

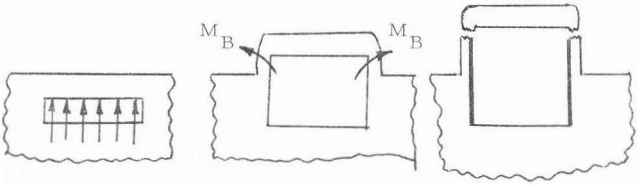

Bending Mode Failure

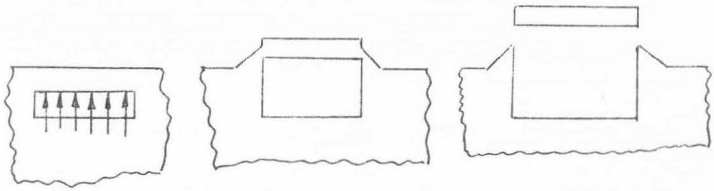

Shearing Mode Failure

Figure A19. Tear burr modes of failure.

Appendix B

Burr Measurement Data

Table B1. Results of turning tests[a]

Order of Cut	SCEA (Degrees)	Depth of cut (inch x 10^{-3})	Feedrate (ipr)	Burr properties[c] Length (inch x 10^{-4})	Thickness (inch x 10^{-4})	Comment
1	17 1/2	40	0.0021	4, 0, 8		
2	↑	70	"	4, 3, 7		Slight BUE on tool
3		100	"	11, 16, 15	8	" " " "
4		40	0.0043	9, 6, 7		" " " "
5		70	"	1, 1,		
6		100	"	24, 19, 21	10, 12	
7		40	0.0065	7, 4, 3		
8	↓	70	"	1, 0, 1		
9	17 1/2	100	"	4, 4, 2	12, 16	
10	0	40	0.0021	300, 350, 400		New insert, no BUE on tool
11	↑	40	"	700, 650, 500		
12[b]		40	"	750, 800, 750		
13[b]	↓	70	"	200, 100, 200		

Table B1. Continued

Order of Cut	SCEA (Degrees)	Depth of cut (inch x 10^{-3})	Feedrate (ipr)	Burr properties[c] Length (inch x 10^{-4})	Burr properties[c] Thickness (inch x 10^{-4})	Comment
14	↓	100	"	600, 400, 400	4, 40	Chip is red hot
15		40	0.0043	600, 750, 700		
16	↓	70	"	400, 400, 150		
17	0	100	0.0043	43, 25, 28	12, 24	
18	↕	40	0.0065	300, 100, 200		No BUE on tool or chip
19	↕	70	"	500, 150, 120		" " " " " "
20	0	100	"	750, 800, 700	56, 72	Chip is red hot
21	-17 1/2	60	0.0021	7, 5, 2		
22[b]	↑	40	"	750, 800, 750		New insert
23	↑	70	"	850, 750, 800	40	Chip is red hot
24	↑	100	"	600, 650, 700	650*(360T)[d], 780*(420T)	" " " "
25	↓	40	0.0043	1300, 1000, 800		
26	-17 1/2	70		400, 350, 400		
27	17 1/2	40	0.0032	300, 450, 400		

Table B1. Continued

Order of Cut	SCEA (Degrees)	Depth of cut (inch x 10^{-3})	Feedrate (ipr)	Burr properties[c] Length (inch x 10^{-4})	Burr properties[c] Thickness (inch x 10^{-4})	Comment
27	17 1/2	40	0.0032	300, 450, 400		
28	"	40	"	0, 0, 0		New insert installed before cutting
29	"	70	"	0, 0, 0	0	
30	"	100	"	0, 0, 0		
31	0	40	0.0032	500, 500, 500		
32	0	70	0.0032	50, 50, 50		
33	"	100	"	300, 300, 300	128*(40T, 108*(40T)	
34	-17 1/2	40	0.0021	500, 550, 500		Faced radially out at end of cut
35		40	"	400, 400, 400		Faced radially out at end of cut
36		40	"	750, 700, 750		
37		70	"	750, 750, 750		Red hot chip
38		100	"	1000, 1000, 1000	580*(400T), 630*(510T)	Red hot chip

Table B1. Continued

Order of Cut	SCEA (Degrees)	Depth of cut (inch x 10^{-3})	Feedrate (ipr)	Burr properties[c] Length (inch x 10^{-4})	Thickness (inch x 10^{-4})	Comment
39	-17 1/2	40	0.0032	1000, 1000, 1000		
40		70	"	600, 600, 600		
41		100	"	500, 500, 500	710*, 570*	
42		40	0.0043	1000, 900, 1000		New insert installed
43		70	"	450, 500, 500		
44		100	"	500, 500, 500	436*(160T), 370*	
45		40	"	600, 600, 600		
46	-17 1/2	40	0.0021	750, 750, 750		Faced out radially (-14° back rake)
47	0	40	0.0021	150, 200, 100	32	(-14° back rake, -4.3° true rake)
48	17 1/2	40	0.0021	7, 12, 7	16, 8	(-14° back rake, -4.3° true rake)
49	-17 1/2	40	0.0021	1100, 1150, 1100	88* (40T)	(-14° back rake)
50	17 1/2	40	0.0021	17, 7, 18		(-14° back rake, Red hot chip)

Table B1. Continued

Order of Cut	SCEA (Degrees)	Depth of cut (inch x 10^{-3})	Feedrate (ipr)	Burr properties[c] Length (inch x 10^{-4})	Thickness (inch x 10^{-4})	Comment
51	17 1/2	40	0.0021	3, 3, 3	12	(+15° true rake)
52	0	40	"	32, 24, 39	28, 20	(+15° true rake)
53	-17 1/2	40	"	600, 600, 600	28	(+15° true rake)

[a] 303 Se stainless steel workpiece, 1/2 inch dia., 1800 RPM. Tool is Kennametal, style VNMP carbide insert with 1/32 nose radius (5° rake unless otherwise noted). Any BUE on tool was removed before making subsequent cuts.
[b] Although no BUE is visable on the tool, the chips indicate that BUE is forming. Chips are continuous.
[c] Multiple entries indicate that more than one measurement was taken.
[d] Values in parentheses indicate burr is triangular at base. T implies typical average width; an asterisk implies actual width at base.

Table B2. End Milling Test Conditions[a]

Seq. No.	Profiling cut		
	Cutter dia. (inch)	Radial Depth of cut (inch)	Feed per tooth (ipn/t)
1	0.250	.1 Dia	0.0005
2	0.250	.1 Dia	0.0033
3	0.250	.1 Dia	0.0020
4		.35 Dia	0.0020
5		.35 Dia	0.0033
6		.35 Dia	0.0005
7		.60 Dia	0.0005
8		.60 Dia	0.0033
9	0.250	.60 Dia	0.0020
10	0.125	.1 Dia	0.0020
11		.1 Dia	0.0033
12		.1 Dia	0.0005
13		.35 Dia	0.0005
14		.35 Dia[b]	0.0033
15		.35 Dia[b]	0.0020
16		.60 Dia[b]	0.0020
17		.60 Dia[b]	0.0033
18	0.125	.60 Dia[b]	0.0005
19	0.375	.1 Dia	0.0005
20		.1 Dia[b]	0.0033
21		.1 Dia	0.0020
22		.35 Dia	0.0020

Table B2. Continued

Seq. No.	Profiling cut: Cutter dia. (inch)	Profiling cut: Radial Depth of cut (inch)	Profiling cut: Feed per tooth (ipn/t)
23	0.375	.35 Dia[b]	0.0033
24	↑	.35 Dia	0.0005
25	‖	.60 Dia	0.0005
26	‖	.60 Dia[b]	0.0033
27	‖	.60 Dia	0.0020
28	‖	1.0 x Dia[c]	0.0005
29	‖	↑ [c]	0.0012
30	‖	‖ [c]	0.0020
31	‖	‖ [c]	0.0020
32	‖	‖ [c]	0.0033
33	‖	‖ [c]	0.0033
34	‖	‖	0.0012
35	↓	↓	0.0005
36	0.375	1.0 x Dia	0.0020

[a] Four flute end mills turning at 1240 RPM and taking a 1/4 inch axial depth of cut.
[b] An axial depth of cut of 0.050 inch was taken on these specimen to prevent cutter breakage.
[c] These cuts are blind slots.

Table B3. Measured burr length[a]. End milling tests - 303 Se workpiece

Seq. No.	Burr location number									
	1	2	3	4	5	6	7	8	9	10
1	13,10,7	-	750,600,650	-		4,3,3	-			-
2	3,5,5,	-	200,250,250	-		2,2,1,	-			-
3	5,11,9	-	200,250,300	-		3,3,3	-			-
4	10,13,9	-	750,750,750	-	12,19,19	3,2,3	-	3,5,5,	15,20,25	-
5	8,12,8	-	750,750,750	-	28,22,28	1,1,1	-	6,3,6		-
6	15,28,21	-	800,750,750	-	21,16,24	3,3,3	-	3,1,1	15,14,20	-
7	32,46,37	-	1450,1500,1450	-	24,12,15	4,3,1	-	11,9,7	20,25,20	-
8	19,13,11	-	1400,1600,1500	-	23,26,29	1,2,1	-	12,9,15		-
9	23,30,17	-	1580,1500,1600	-	22,14,16	0,0,0	-	8,9,9	28,20,36	-
10	1,2,1	-	120,150,100	-		1,2,2	-			-
11	0,0,0	-	350,300,400	-		2,0,0	-			-
12	3,5,5	-	600,650,600	-		1,1,1	-			-
13	6,7,5	-	400,420,450	-	19,24,14	2,1,1	-	3,5,4		-
14	10,5,10	-	320,350,300			4,3,2	-			-
15	1,1,1	-	320,350,350	-		3,1,1	-			-
16	13,11,12	-	750,720,800	-		2,1,1	-	10,14,15		-
17	20,25,21	-	750,720,950	-		1,2,1	-			-
18	8,10,8	-	740,800,850	-	24,25,24	2,2,1	-	13,5,12		-
19	11,16,16	-	300,350,350	-		1,2,1	-			-
20	8,10,8	-	300,320,350	-		1,1,2	-			-
21	6,5,4	-	400,450,450	-		1,2,2,	-			-
22	6,6,4	-	1400,1420,1400	-	24,29,29	2,2,1	-	8,2,5	36,33,22	-
23	1,3,5	-	100,50,150	-	42,40,43	1,1,1	-	3,7,2		-
24	13,16,18	-	1050,1100,1100	-	20,33,29	3,2,2	-	9,8,12	25,25,37	-
25	14,14,19	-	2200,2100,2200	-	34,43,22	1,2,4	-	10,8,6	22,20,45	

Table B3. Continued

Seq. No.	Burr location number 1	2	3	4	5	6	7	8	9	10
26	5,5,10	-	2300,2250,2250	-	30,32,15	4,5,5	-	13,8,9		-
27	5,7,3	-	2450,2500,2450	-	38,38,29	2,1,2	-	15,10,2	55,59,60	-
28	15,17,11	11,18,20	-	-	-	3,2,4	27,42,38	11,13,10	-	14,15,20
29	8,15,13	9,3,10	-	-	-	3,1,2	80,90,80	25,14,3	-	12,25,13
30	30,10,10	25,25,20	-	-	-	2,2,4	70,80,80	70,80,80	-	50,40,40
31	29,26,20	44,36,29	-	-	-	6,2,1	80,80,90	80,80,90	-	18,11,24
32	25,24,27	27,23,23	-	-	-	4,2,13	160,140, 150	37,12,6	-	15,21,22
33	42,21,10	47,43,49	-	-	-	2,7,1	31,24,30	21,15,7	-	1,3,3
34	6,11,4	13,15,12	2600,2500, 2400	0,0,1	29,38,18	1,3,2	22,31,51	26,9,4	-	-
35	18,11,15	11,24,11	2100,2200, 2300	1,2,1	22,23,19	1,0,1	42,53,50	16,16,2	-	-
36	26,27,12	33,27,15	2400,2500, 2400	1,0,1	15,31,34	1,2,1	25,31,29	25,16,4	-	-

[a] Values shown are burr thickness in .0001 inch units. Three measurements were taken at each condition.

Table B3. Measured burr length*. End milling tests - 303 Se workpiece

Seq. No.	Burr location number									
	1	2	3	4	5	6	7	8	9	10
1	13,10,7	-	750,600,650	-		4,3,3,	-			-
2	3,5,5,	-	200,250,250	-		2,2,1	-			-
3	5,11,9	-	200,250,300	-		3,3,3,	-			-
4	10,13,9	-	750,750,750	-	12,19,19	3,2,3,	-	3,5,5,	15,20,25	-
5	8,12,8	-	750,750,750	-	28,22,28	1,1,1	-	6,3,6		-
6	15,28,21	-	800,750,750	-	21,16,24	3,3,3	-	3,1,1	15,14,20	-
7	32,46,37	-	1450,1500,1450	-	24,12,15	4,3,1	-	11,9,7	20,25,20	-
8	19,13,11	-	1400,1600,1500	-	23,26,29	1,2,1	-	12,9,15		-
9	23,30,17	-	1580,1500,1600	-	22,14,16	0,0,0	-	8,9,9	28,20,36	-
10	1,2,1	-	120,150,100	-		1,2,2	-			-
11	0,0,0	-	350,300,400	-		2,0,0	-			-
12	3,5,5,	-	600,650,600	-		1,1,1	-			-
13	6,7,5	-	400,420,450	-	19,24,14	2,1,1	-	3,5,4		-
14	10,5,10	-	320,350,300			4,3,2	-			-
15	1,1,1	-	320,350,350	-		3,1,1	-			-
16	13,11,12	-	750,720,800	-		2,1,1	-	10,14,15		-
17	20,25,21	-	750,720,950	-		1,2,1	-			-
18	8,10,8	-	750,800,850	-	24,25,24	2,2,1	-	13,5,12		-
19	11,16,16	-	300,350,350	-		1,2,1	-			-
20	8,10,8	-	300,320,350	-		1,1,2	-			-
21	6,5,4	-	400,450,450	-		1,2,2	-			-
22	6,6,4	-	1400,1420,1400	-	24,29,29	2,2,1	-	8.2,5	36,33,22	-
23	1,3,5	-	100,50,150	-	42,40,43	1,1,1	-	3,7,2		-
24	13,16,18	-	1050,1100,1100	-	20,33029	3,2,2	-	9,8,12	25,25,37	-
25	14,14,19	-	2200,2100,2200	-	34,43,22	1,2,4	-	10,8,6	22,20,45	
26	5,5,10	-	2300,2250,2250	-	30,32,15	4,5,5	-	13,8,9		-
27	5,7,3	-	2450,2500,2450	-	38,38,29	2,1,2	-	15,10,2	55,59,60	-
28	15,17,11	11,18,20	-	-	-	3,2,4	27,42,38	11,13,10	-	14,15,20
29	8,15,13	9,3,10	-	-	-	3,1,2	80,90,80	25,14,3	-	12,25,13

Table B4. Measured burr thickness[a]. End milling tests - 303 Se workpiece

Seq. No.	Burr location number									
	1	2	3	4	5	6	7	8	9	10
1	-0	-		-			-			-
2	20	-		-			-			-
3	-0	-		-			-			-
4	-0	-		-			-			-
33	0									-
34	0		12				4			-
35	0		12	8			12			-
36	0			0			16			-

[a] Values shown are burr thickness in .0001 inch units.

Table B5. Measured burr lengths[a]. Side milling tests - 303 Se workpiece

Seq. No.	Burr location number							
	1	2	3	4	5	6	7	8
1	44,25,25	55,32,22	70,80,60	22,17,12	25,19,15	3,1,2	6,3,4	15,15,11
2	25,22,24	25,34,24	60,36,39	31,30,48	57,46,43	4,6,3	8,7,3	1,2,1
3	25,30,25	18,55,38	50,56,50	55,59,52	2,2,4	1,0,4	3,1,1	6,1,1
4	25,21,27	19,16,17	70,170,70	50,30,110	250,250,270	5,10,3	7,11,4	5,2,3
5	27,40,40	30,40,40	70,60,50	180,120,40	600,630,590	5,2,1	1,1,3	1,0,2
6	32,47,33	27,32,29	90,80,50	50,60,60	3000,3200,3150	1,10,5	3,1,7	5,5,4
7	29,27,29	17,18,25	110,60,250	70,70,80	600,650,550	0,2,0	5,4,4	3,1,3
8	36,20,34	16,19,21	70,70,70	100,80,80	850,900,900	5,3,4	2,3,1,	3,5,4

[a]Values shown are burr length in .0001 inch units. Three readings were taken of each burr.

Table B6. Measured burr lengths. Grinding burrs - 303 Se workpiece

Seq. No.	Machining Conditions: Depth of cut	Machining Conditions: No. of passes made across part	Burr location: 1	2	3	4
1	.0005	10	37,33,21	18,22,46	27,12,2	4,1,5
2	.0002	1	10,10,15	20,5,14	29,0,0	8,11,0
3	.0015	10	0,0,0	45,37,35	55,60,70	3,2,3
4	.0010	1	7,10,22	8,2,6	51,16,14	0,0,0
5	.0010	10	50,100,30	100,100,100	30,29,31	1,5,1
6	.0005	1	15,3,5	1,0,0	28,8,10	0,0,16

Values shown are in .0001 inch units. Wheel used was a PA46-H8-V40 wheel (7" dia). A water soluble coolant was used.

Table B7. Measured burr lengths and thicknesses. Drilling burrs - 303 Se workpiece

Seq. No.	Burr length		Burr thickness	
	Top burr	Bottom burr	Top burr	Bottom burr
1	4,7,8 8,6,14 7,9,13	2,2,7 13,31,41 50,30,50	-	-
2	4,1,15 6,3,11 15,5,2	60,90,110 80,90,90 90,80,14	24*	12,48
3	36,35,22 23,26,21 10,14,15	15,17,22 18,11,16	16*,20	24*,12
4	11,14,20 9,14,16 10,6,8	26,6,22 21,15,22 46,43,6	16*	8,16*
5	-	-	-	-
6	14,6,11 21,18,9	25,11,18 10,17,13	-	20*(12T),16
7	20,17,21 22,24,23 24,21,26	24,36,40 12,12,23	28*,72*	32,40*(20T)
8	22,20,18 15,16,23 15,20,21	25,14,35 16,30,20 30,35,30	28,64*	32,40

Table B7. Continued

Seq. No.	Burr length		Burr thickness	
	Top burr	Bottom burr	Top burr	Bottom burr
9	23,25,24 3,3,6 29,20,22	7,8,7 4,3,4, 34,10,42	8	16,24*
10	1,20,21 21,28,20 12,19,6 1,20,18	22,7,45 27,57,53 45,70,90 90,30,40	-	16,20
1W	7,5,3	50,10,300	12	48
10W	2,17,5	100,50,70	24	12,16
15W	10,7,4	57,17,56		
20W	11,6,2	26,41,20	16,20	16,8
25W	10,4,3	31,100,70	8,40	16,16

Values shown are burr size in 0.0001 inch units. W indicates holes from the drill wear test. Each line of data represents data from one hole (in general three holes were drilled at each combination). Values with asterisks indicate that the burr is tringular shaped and that the value listed is taken at the base of the burr. Values which are more typical of burr width are followed by a 'T'. Thickness values shown are from one hole only.

Appendix C

Analysis of Variance Results

Table C1. Analysis of variance. Turning-burr lengths

Source of variation	DF	Sum of squares	Mean squares	Variance ratio
A SCEA	2	70663.6402469	35331.8201235	2370.*
B FEED	2	719.0417284	359.5208642	24.2*
C DEPTH	2	7814.3054321	3907.1527160	263*
AB	4	887.6316049	221.9079012	15.*
AC	4	4710.2967901	1177.5741975	80.*
BC	4	5352.7708642	1338.1927160	91.*
ABC	8	3469.4780247	433.6847531	29.3*
Total	80	94419.7446914	1180.2468086	
Error	54	802.5800000	14.8625926	

$F_{.05} = 3.15$ $(\nu_1=2, \nu_2=60)$
$F_{.05} = 2.53$ $(\nu_1=4, \nu_2=60)$
$F_{.05} = 2.10$ $(\nu_1=8, \nu_2=60)$

Significance at the 5 percent level is indicated by an asterisk. Data for this analysis is based on a 5° true rake tool, and the following feedrates: .0021, .0032, .0043.

Table C2. Analysis of variance. End mill - Burr #1 length

Code	Source of variance	DF	Sum of squares	Mean squares	Variance ratio
A	Diameter	2	10.84	5.42	59.8*
B	Depth	2	14.33	7.17	78.6*
C	Feedrate	2	8.04	4.02	44.2*
AB	Interaction	4	7.77	1.94	21.3*
AC	"	4	7.87	1.97	21.7*
BC	"	4	.38	.09	--
ABC	"	8	5.69	.71	7.75*
	Error	54	4.90	.091	
	Total	80	59.82		

$F_{.05} = 3.15$ $(\nu_1 = 2, \nu_2 = 60)$
$F_{.05} = 2.53$ $(\nu_1 = 4, \nu_2 = 60)$
$F_{.05} = 2.10$ $(\nu_1 = 8, \nu_2 = 60)$

Table C3. Analysis of variance. End mill - burr # 3 length

Code	Source of variance	DF	Sum of squares	Mean squares	Variance ratio
A	Diameter	2	61,129	30,564	1,390*
B	Depth	2	197,568	98,784	4,490*
C	Feedrate	2	5,443	2,722	123*
AB	Interaction	4	54,398	13,600	620*
AC	"	4	10,594	2,649	120*
BC	"	4	9,114	2,279	104*
ABC	"	8	11,889	1,486	68*
	Error	54	1,194	22.11	
	Total	80	351,331		

$F_{.05} = 3.15$ ($\nu_1=2$, $\nu_2=60$)
$F_{.05} = 2.53$ ($\nu_1=4$, $\nu_2=60$)
$F_{.05} = 2.10$ ($\nu_1=8$, $\nu_2=60$)

Table C4. Analysis of variance. End mill - burr # 5 length

Code	Source of variance	DF	Sum of squares	Mean squares	Variance ratio
A	Diameter	1	9.88	9.88	28.2*
B	Depth	1	.43	.43	--
C	Feedrate	1	.007	.007	--
AB	Interaction	1	.96	.96	--
AC	"	1	.107	.107	--
BC	"	1	.135	.135	--
ABC	"	1	.015	.015	--
	Error	16	5.593	.350	
	Total	23	17.125		

$F_{.05} = 4.49$ ($\nu_1=1$, $\nu_2=16$)

Table C5. Analysis of variances. End mill - burr # 6 length

Code	Source of variance	DF	Sum of squares	Mean squares	Variance ratio
A	Diameter	2	.0491	.0246	4.82*
B	Depth	2	.0069	.0035	--
C	Feedrate	2	.0254	.0127	2.5
AB	Interaction	4	.2212	.0553	11.0*
AC	"	4	.1294	.0323	6.35*
BC	"	4	.1360	.0340	6.68*
ABC	"	8	.1736	.0217	4.27*
	Error	54	.2733	.0051	
	Total	80	1.015		

$F_{.05} = 3.15$ $(\nu_1=2, \nu_2=60)$
$F_{.05} = 2.53$ $(\nu_1=4, \nu_2=60)$
$F_{.05} = 2.10$ $(\nu_1=8, \nu_2=60)$

Table C6. Analysis of variance. End milling - burr # 8 length

Code	Source of variance	DF	Sum of squares	Mean squares	Variance ratio
A	Diameter	1	.240	.240	2.86
B	Depth	1	.735	.735	8.74*
C	Feedrate	1	.007	.007	--
AB	Interaction	1	.327	.327	3.89
AC	"	1	.135	.135	--
BC	"	1	.027	.027	--
ABC	"	1	.282	.282	3.35
	Error	16	1.346	.084	
	Total	23			

$F_{.05} = 4.49$ $(\nu_1=1, \nu_2=16)$

Table C7. Analysis of variance. End milling - burr #9 length

Code	Source of variance	DF	Sum of squares	Mean squares	Variance ratio
A	Diameter	1	13.65	13.65	26.8*
B	Depth	1	6.30	6.30	12.4*
C	Feedrate	1	6.10	6.10	12.0*
AB	Interaction	1	.77	.77	--
AC	"	1	1.55	1.55	--
BC	"	1	3.45	3.45	6.78*
ABC	"	1	2.34	2.34	4.59*
	Error	16	8.2	.51	
	Total	23	42.37		

$F_{.05} = 4.49$ (ν_1=1, ν_2=16)

Table C8. Analysis of variance. Side milling - burr # 1 length

Code	Source of variance	DF	Sum of squares	Mean squares	Variance ratio
A	Helix angle	1	2.41	2.41	5.62*
B	Depth	1	1.31	1.31	3.05
C	Feedrate	1	.16	.16	--
AB	Interaction	1	.43	.43	1.0
AC	"	1	.67	.67	--
BC	"	1	.11	.11	--
ABC	"	1	.11	.11	--
	Error	16	6.89	.43	
	Total	23	12.08		

$F_{.04} = 4.49$ (ν_1=1, ν_2=16)

Table C9. Analysis of variance. Side milling - burr # 2 length

Code	Source of variance	DF	Sum of squares	Mean squares	Variance ratio
A	Helix angle	1	.70	.70	--
B	Depth	1	5.13	5.13	5.62*
C	Feedrate	1	5.13	5.13	5.62*
AB	Interaction	1	1.17	1.17	--
AC	"	1	1.45	1.45	--
BC	"	1	.09	.09	--
ABC	"	1	1.08	1.08	--
	Error	16	14.54	.91	--
	Total	23	29.31		

$F_{.05} = 4.49$ $(\nu_1=1, \nu_2=16)$

Table C10. Analysis of variance. Side milling - burr # 3 length

Code	Source of variance	DF	Sum of squares	Mean squares	Variance ratio
A	Helix angle	1	19.98	19.98	--
B	Depth	1	51.33	51.33	2.98
C	Feedrate	1	3.45	3.45	--
AB	Interaction	1	4.95	4.95	--
AC	"	1	.67	.67	--
BC	"	1	.18	.18	--
ABC	"	1	95.6	95.6	5.5*
	Error	16	276.99	17.31	
	Total	23	478.33		

$F_{.05} = 4.49$ $(\nu_1=1, \nu_2=16)$

Table C11. Analysis of variance. Side milling - burr #4 length

Code	Source of variance	DF	Sum of squares	Mean squares	Variance ratio
A	Helix angle	1	93.62	93.62	10.6*
B	Depth	1	11.48	11.48	--
C	Feedrate	1	.96	.96	--
AB	Interaction	1	21.28	21.28	--
AC	"	1	18.73	18.73	--
BC	"	1	12.91	12.91	--
ABC	"	1	24.81	24.81	2.83
	Error	16	140.13	8.76	
	Total	23	323.91		

$F_{.05} = 4.49$ (ν_1=1, ν_2=16)

Table C12. Analysis of variance. Side milling - burr #5 length

Code	Source of variance	DF	Sum of squares	Mean squares	Variance ratio
A	Helix angle	1	89,304	89,304	9.2*
B	Depth	1	15,728	15,728	--
C	Feedrate	1	35,466	35,466	3.62
AB	Interaction	1	22,179	22,179	--
AC	"	1	23,650	23,650	--
BC	"	1	15,010	15,010	--
ABC	"	1	22,558	22,558	2.32
	Error	16	224,193	9747.	
	Total	23	224193.		

Table C13. Analysis of variance. Side milling - burr #6 length

Code	Source of variance	DF	Sum of squares	Mean square	Variance ratio
A	Helix angle	1	.007	.007	--
B	Depth	1	.015	.015	--
C	Feedrate	1	.602	.602	10.0*
AB	Interaction	1	.082	.082	--
AC	"	1	.002	.002	--
BC	"	1	.027	.027	--
ABC	"	1	.007	.007	--
	Error	16	.95	.060	
	Total	23	1.69		

Table C14. Analysis of variance. Side milling - burr #7 length

Code	Source of variance	DF	Sum of squares	Mean square	Variance ratio
A	Helix angle	1	.220	.220	5.*
B	Depth	1	.0004	.0004	--
C	Feedrate	1	.184	.184	4.18*
AB	Interaction	1	.020	.020	--
AC	"	1	.220	.220	5.*
BC	"	1	.0004	.0004	--
ABC	"	1	.260	.260	5.9*
	Error	16	.70	.044	
	Total	23	1.61		

Table C15. Analysis of variance. Side milling - burr #8 length

Code	Source of variance	DF	Sum of squares	Mean square	Variance ratio
A	Helix angle	1	.304	.304	12.1*
B	Depth	1	.260	.260	10.4*
C	Feedrate	1	.150	.150	6.0*
AB	Interaction	1	.350	.350	14.0*
AC	"	1	1.084	1.084	43.3*
BC	"	1	.454	.454	18.2*
ABC	"	1	.844	.844	34.0*
	Error	16	.400	.025	
	Total	23	3.85		

Table C16. Analysis of variance. Drilling - Top burr length

Code	Source of variance	DF	Sum of squares	Mean square	Variance ratio
A	Helix angle	1	6.42	6.42	20.6*
B	Point angle	1	8.33	8.33	26.8*
C	Feedrate	1	5.61	5.61	18.00*
AB	Interaction	1	1.36	1.36	4.38*
AC	"	1	0.03	0.03	--
BC	"	1	.26	.26	.86
ABC	"	1	1.90	1.90	6.1*
	Error	64	19.98	3.12	
	Total	71	43.90		

$F_{.05} = 4.0$ ($\nu_1=1$, $\nu_2=60$)

Table C17. Analysis of variance. Drilling - Bottom burr length

Code	Source of variance	DF	Sum of squares	Mean square	Variance ratio
A	Helix angle	1	4071.03	4071.03	151.0*
B	Point angle	1	331.96	331.96	12.3*
C	Feedrate	1	198.67	198.67	7.36*
AB	Interaction	1	1008.00	1008.00	37.*
AC	"	1	2.14	2.14	.08
BC	"	1	34.72	34.72	1.28
ABC	"	1	16.06	16.06	.59
	Error	64	1729.10	27.02	
	Total	71	7391.68		